EPA U.S. Environmental Protection Agency
Office of Research and Development

Industrial Environmental Research
Laboratory
Research Triangle Park, North Carolina 27711

EPA-600/7-77-132
November 1977

DEVELOPMENT OF A HIGH-TEMPERATURE/HIGH-PRESSURE ELECTROSTATIC PRECIPITATOR

Interagency
Energy-Environment
Research and Development
Program Report

RESEARCH REPORTING SERIES

Research reports of the Office of Research and Development, U.S. Environmental Protection Agency, have been grouped into seven series. These seven broad categories were established to facilitate further development and application of environmental technology. Elimination of traditional grouping was consciously planned to foster technology transfer and a maximum interface in related fields. The seven series are:

1. Environmental Health Effects Research
2. Environmental Protection Technology
3. Ecological Research
4. Environmental Monitoring
5. Socioeconomic Environmental Studies
6. Scientific and Technical Assessment Reports (STAR)
7. Interagency Energy-Environment Research and Development

This report has been assigned to the INTERAGENCY ENERGY-ENVIRONMENT RESEARCH AND DEVELOPMENT series. Reports in this series result from the effort funded under the 17-agency Federal Energy/Environment Research and Development Program. These studies relate to EPA's mission to protect the public health and welfare from adverse effects of pollutants associated with energy systems. The goal of the Program is to assure the rapid development of domestic energy supplies in an environmentally--compatible manner by providing the necessary environmental data and control technology. Investigations include analyses of the transport of energy-related pollutants and their health and ecological effects; assessments of, and development of, control technologies for energy systems; and integrated assessments of a wide range of energy-related environmental issues.

REVIEW NOTICE

This report has been reviewed by the participating Federal Agencies, and approved for publication. Approval does not signify that the contents necessarily reflect the views and policies of the Government, nor does mention of trade names or commercial products constitute endorsement or recommendation for use.

This document is available to the public through the National Technical Information Service, Springfield, Virginia 22161.

EPA-600/7-77-132
November 1977

DEVELOPMENT OF A HIGH-TEMPERATURE/HIGH-PRESSURE ELECTROSTATIC PRECIPITATOR

by

J.R. Bush, P.L. Feldman, and M. Robinson

Cottrell Environmental Systems
Research-Cottrell, Inc.
Bound Brook, New Jersey 08805

Contract No. 68-02-2104
Program Element No. EHE623A

EPA Project Officer: Leslie E. Sparks

Industrial Environmental Research Laboratory
Office of Energy, Minerals, and Industry
Research Triangle Park, N.C. 27711

Prepared for

U.S. ENVIRONMENTAL PROTECTION AGENCY
Office of Research and Development
Washington, D.C. 20460

ABSTRACT

The feasibility of electrostatic precipitation at temperatures and pressures varying from room conditions to 1366 K and 3550 kPa, respectively, has been demonstrated in a laboratory wire-pipe electrode system. Subject to appropriate choices of polarity and pressure, stable corona discharges are obtained at all temperatures. Current-voltage characteristics for both polarities are reported for dry air, a simulated combustion gas, and a substitute fuel gas. The effects of temperature, pressure, and electrode geometry on sparkover voltage, corona-starting voltage and current are evaluated. It is recommended that this study be extended to pilot coal gasifiers and fluidized-bed combustors to obtain detailed design data, and permit determination of collection efficiencies and precipitate characteristics under actual operating conditions. A preliminary cost estimate is presented for a precipitator intended for use in connection with a commercial fluidized-bed combustor and turbine system.

EXECUTIVE SUMMARY

At the elevated temperatures and pressures characteristic of many advanced coal-conversion processes, electrostatic precipitators exhibit potentially higher particle-collecting efficiencies than prevail under conventional conditions of precipitator application. High efficiencies are an anticipated consequence of the increased voltages that can be applied to the precipitator over broad pressure/temperature ranges of practical interest. This efficiency effect is unique for precipitators. In other particulate collection devices, efficiency generally decreases with increasing temperature and pressure. But even for precipitators, it must be remembered that improved performance is not an unvarying consequence of high pressure and temperature. Beneficial results depend on suitably combining the two variables.

Current-voltage characteristics and sparkover data for both positive and negative polarities are reported here for three gas mixtures: dry air, a simulated flue gas, and a substitute (noncombustible) fuel gas.

In the present study, no practical upper limit is reached for stable corona at temperatures and pressures as high as 1366 K (2000°F) and 3550 kPa (515 psia). In some instances, however, limits imposed by the critical pressure are approached. The critical pressure is the lowest elevated pressure at which corona starting and sparkover voltages coincide and beyond which a stable corona is not possible.

Increasing the temperature raises the critical pressure and so results in a broader operating range of pressure. The negative-corona critical pressure, attained here only at room temperature, is found to be significantly higher than the positive value. In other words, the pressure range over which negative corona is possible is greater than the range for positive corona.

Positive sparkover voltage exceeds negative for conditions of low gas density and high temperature. For high density, negative sparkover is higher than positive sparkover.

The amplitude of discharge-electrode oscillations is found to be dependent on electrode length, shape, tension and material. Short, rigid or high stressed electrodes produced minimal oscillation. The rigors of high-temperature service require discharge and collecting electrodes of high tensile strength and high oxidation and carburization resistance. Oxidation and carburization result in an expanding scale growth that effects both corona-starting and sparkover voltages. Inconel 601 performs satisfactorily at temperatures at least to 1366 K (2000°F).

A preliminary cost estimate is presented for a precipitator intended for use in connection with a commercial fluidized-bed combustor and turbine system.

In view of the encouraging results obtained so far--but which are limited to a particle-free system--it is recommended that we next proceed to the design and operation of a pilot precipitator treating fluidized-bed combustor or gasifier effluents.

CONTENTS

	Page
Abstract	ii
Executive Summary	iii
Figures	vii
Tables	ix
Nomenclature	x
Acknowledgments	xii
1. Introduction	1
Objectives and Scope	1
Fundamentals of High Temperature/Pressure Precipitation	2
Overview	2
Critical Pressure	3
Thermal Ionization	4
Earlier Studies	6
2. Conclusions	7
3 Recommendations	9
4. Experimental Apparatus and Procedure	10
Test Precipitator	10
High-Voltage Power Supply	12
Temperature Control System	12
Gas-Flow System	15
Test Conditions and Procedure	21
Discharge-Electrode Oscillation Test	22
5. Results and Discussion	25
The Experimental Data	25
Temperature/Pressure Limitations on Corona Stability	25
General Remarks	25
Excessive Current	26
Positive Critical Pressure	26
Negative Critical Pressure	27
Practical Precipitator-Tube Diameter	27
Polarity Effects	28

Page

Background Considerations 28
Experimental Observations in Air 29
Experimental Observations in Combustion and Fuel Gases 29
Corona-Starting Voltage 30
Data Fluctuations 30
Peek's Equation 30
Current-Voltage Elbows 31
Discharge-Electrode Oscillations 32
Material Evaluation 32

6. Commercial Cost Estimate 49
Precipitator Size for Fluidized-Bed Combustion 49
Material-Temperature Dependence 52

7. References 57

8. Appendices 60

A. Calculation of Thermal Conductivity 60
B. Calculation of Ionic Mobility 62
C. Determination of Gas-Mixture Composition 63
D. Components of Power-Supply Circuit 65
E. List of Experimental Precipitator Drawings 66

FIGURES

Number		Page
1	Laboratory Precipitator and Pressure Vessel	11
2	Power Supply and Instrumentation Circuitry	13
3	Three Zone Precipitator Heater and Control System	14
4	Internal Tube and Gas Temperature Calibration to Control System	16
5	Pressurizing and Mixing Flow System to Precipitator	17
6	Humidifier Internal Details	18
7	Overall Test and Control Room Layout Schematic	19
8	Test Apparatus for Electrode Oscillation Studies	23
9	Discharge Electrode Geometries for Oscillation Studies	24
10	Current-Voltage Curves in Air at 294 K, 533 K, and 950 K	36
11	Current-Voltage curves in Air at 811 K	37
12	Current-Voltage Curves in Air at 1089 K	38
13	Current-Voltage Curves in Air at 1366 K	39
14	Current-Voltage Curves for a Simulated Combustion Gas Mixture	40
15	Current-Voltage Curves for a Substitute Fuel Gas Mixture	41
16	Sparking and Corona Starting Voltages in Air at 294 K and 533 K	42

17	Sparking and Corona Starting Voltages in Air at 811 K and 950 K	43
18	Sparking and Corona Starting Voltages in Air at 1089 K and 1366 K	44
19	Sparking and Corona Starting Voltages for a Simulated Combustion Gas	45
20	Sparking and Corona Starting Voltages for a Substitute Fuel Gas	46
21	Negative Corona Starting Fields in Air Compared with Peek's Equation	47
22	Positive Corona Starting Fields in Air Compared with Peek's Equation	48

TABLES

		Page
1.	Test Gas Composition	15
2.	Thermal Conductivity and Mobility of Test Gases	20
3.	Experimental Test Variables	21
4.	Discharge Electrode Geometries	22
5.	Discharge Electrode Oscillation Results	34
6.	Determination of Gas Flow Requirements for a Fluidized Bed Combustor Plant	54
7.	Design Alternatives for a Pressurized Precipitator	54
8.	Cost Estimation for Two Precipitator Designs	55
A-1	Calculated Thermal Conductivity of Test Gas Mixture	61
A-2	Calculated Thermal Conductivity of a Low Btu Fuel Gas	61
B-1	Calculated Ionic Mobilities of Gas Mixtures	62
C-1	Combustion Gas Mixture Composition	63
C-2	Substitute Fuel Gas Mixture Composition	64
D	Components of Power-Supply Circuit	65
E	List of Experimental Precipitator Drawings	66

NOMENCLATURE

b_o^-	negative ion mobility at standard conditions ($m^2/(sec-V)$)
b_o^+	positive ion mobility of gas at standard conditions ($m^2/(sec-V)$)
C_i	capicitator
CR_i	silicon rectifier
D	inside diameter of tube (m)
d	outer diameter of wire (m)
E	electric field at wire surface (V/m)
E_c	corona-starting field at wire surface (V/m)
i	current (A)
j	linear current density (A/m)
k	thermal conductivity of gas (W/m-K))
L_i	inductor
M_i	molecular weight of species i
m	surface roughness factor (dimensionless)
P	pressure
P_o	standard pressure
R_i	resistor
r_i	wire radius (m)
r_o	tube radius (m)
T	temperature (K)

T_o	standard temperature (294 K)
TC	thermocouple sensor
V	voltage (V)
V_c	corona-starting voltage (V)
w	ratio of weight of discharge electrode and tensioning weight to weight of discharge electrode alone (dimensionless)
y_i	mole fraction of component i
δ	relative gas density (dimensionless)
ε_o	permittivity of free space (8.85×10^{-12} F/m)

ACKNOWLEDGEMENTS

The authors are grateful to Messrs. Robert F. Brown, Alex Penyak, III, and Joseph C. Shepard of the staff of Research-Cottrell, Inc. for their numerous contributions to the successful outcome of this study. We are likewise indebted to Dr. Leslie Sparks, EPA Project Officer, for his assistance and helpful comments.

SECTION I

INTRODUCTION

OBJECTIVES AND SCOPE

The objective of this project is to demonstrate the feasibility of electrostatic precipitation at the elevated temperatures and pressures associated with developing coal-conversion processes. In particular, it is desired to

(1) Explore corona stability over a range of temperatures and pressures from room levels to 1366 K and 3550 kPa, respectively.

(2) Estabish current-voltage characteristics (including corona-staring and sparkover voltages), in terms of temperature, pressure, geometry and polarity, in a particle-free test precipitator using dry air, a simulated combustion gas and a substitute fuel gas.

(3) Prepare a preliminary cost estimate for a commercial precipitator to be used in conjunction with a 300-MW pressurized fluidized-bed combustor. Detailed and more accurate estimates must await the availability of particle-collection data.

Technological developments in coal-utilization systems are directed at processes producing (1) heat and electricity through combustion, (2) synthetic fuel gases for local industrial or pipeline use, and (3) liquids and tars for use as chemical feedstocks. Each process operates under characteristic conditions of temperatures, pressure, gas composition, and particulate type. Pressurized fluidized-bed combustion and low-Btu gasification require particulate removal ahead of a gas turbine at temperatures ranging from 950 K to 1400 K and pressures above 700 kPa. In the generation of high-Btu gas, the removal of particulate tar and char usually occurs at temperatures between 500 and 950 K and pressures above 7000 kPa. The particulate-cleanup stage in the gasification system is necessary to protect downstream catalytic processes. Liquefaction processes generate tars and oils that must be separated from a gas phase at temperatures below 500 K and pressures generally below 700 kPa.

The gas-cleaning requirements of the foregoing processes govern the selection of the temperature and pressure ranges and the gas compositions considered in this investigation.

FUNDAMENTALS OF HIGH TEMPERATURE/PRESSURE PRECIPITATION

Overview

The electrostatic precipitator appears to be unique among conventional particulate collectors such as fabric filters, cyclones, and scrubbers, in that elevated gas pressure offers the promise of increased collecting efficiency. Such improvement results from the potentially higher sparkover voltages, and hence greater particle-migration velocities, attainable at high pressures (20). The advantage holds for precipitation at high temperature, as long as this condition occurs in combination with adequate pressure. This important consideration for high-temperature and pressure particulate gas cleaning deserves special mention in view of its lack of emphasis--if not neglect--by recent writers on the subject (4, 5, 18, 37).

There is a fundamental problem encountered either in designing a precipitator for a given high temperature/pressure service, or in making a realistic economic assessment of its merits. This is our incomplete knowledge of i) the range of variables (pressure, temperature, electrode geometry, gas composition, polarity) over which a stable corona discharge can be maintained, and ii) the current-voltage characteristics in that range. In particular, there exists for the positive discharge a critical pressure (not to be confused with its thermodynamic namesake) above which sparkover alone, without antecedent corona, prevails. When the discharge polarity is negative, the critical phenomenon is not so precisely defined, and a post-critical discharge (often unstable) may be found at pressures extending beyond the critical value.

Thus, in either polarity, the critical pressure effectively sets a pressure limit on conventional electrostatic precipitation. The practical consequences of this limitation are, however, not likely to be serious, for the critical pressure is susceptible to control. Available data indicate this range of control to be so broad in practice that the elimination of critical problems, at any presently foreseeable temperature/pressure combination, should not be difficult, but only insofar as the dependence of the discharge on its governing variables is known.

This study represents the first reported attempt, at any pressure, to establish a corona discharge suitable for electrostaic precipitation at as high a gas temperature as 1360 K, 1200 K being the earlier maximum (3). The highest pressure at which a precipitator has ever operated is 5500 kPa (at outdoor temperature) (11), exceeding the present maximum of 3550 kPa.

If pressure presents no insurmountable barrier to the precipitation process, at least in terms of currently anticipated applications, neither does temperature, as long as the two variables appropriately complement one another. Again, since high-temperature precipitation (as opposed to hot precipitation (35) will usually be accompanied by elevated pressure, loss of corona stability by reason of temperature is not expected to constitute a general problem. However, at temperatures beyond those herein contemplated, thermal ionization must ultimately be supposed to set an upper limit to stable electrostatic precipitation.

Critical Pressure

It is a well-known fact that an increase in gas pressure in the neighborhood of atmospheric will raise the breakdown voltage for electrode systems of both parallel-plate and corona-discharge geometries. Less familiar are the contrary effects produced by much lower or higher pressures. Thus, the breakdown voltage drops as the pressure falls below atmospheric, passing through a minimum at pressures of the order of 100 Pa. The minimum occurs because the number of gas molecules in the interelectrode gap is proportional to the pressure. Low pressure results in a long mean free path and, consequently, few electrons, in traversing the gas, manage to collide with gas molecules and ionize them. In order to have sufficient ionization to lead to breakdown, the accelerating electric field and, hence, the applied voltage, must compensate for the low-density effect. The less the pressure below a certain value, the higher, then, is the voltage level required for breakdown. However, as the pressure rises away from its minimum voltage value, the mean free path decreases. Although electron-molecule collisions are now more frequent, few electrons are able to acquire sufficient kinetic energy over the reduced mean free path to ionize gas molecules by collision. It follows that in order to generate enough ionization in the gap, the voltage must be raised together with the gas pressure. This relation holds until the neighborhood of the critical pressure is approached. (We note, in passing, that low-pressure (to ∿300 Pa) electrostatic precipitation has been employed in connection with stratospheric aerosol sampling (20)).

The earliest observations bearing on the critical pressure were made by Ryan (24) and his student Ekert (10) at the beginning of this century. Later workers showed that for electronegative gases, as the pressure is raised above atmospheric for a positive-corona system, a point is reached at which sparkover is <u>not</u> preceded by corona. In other words, although both the corona-starting and sparkover voltages initially increase with pressure above atmospheric, eventually the difference between the two voltages begins to narrow, and ultimately they coincide. The pressure at this point of intersection, beyond which a positive corona discharge is impossible, is termed the critical pressure.

A negative critical pressure, i.e., a critical pressure for negative corona (at first though not to exist), was discovered recently by Robinson (20) using combinations of electrode geometries and pressures not employed by earlier investigators. The negative critical pressure differs from the positive in that the former is not so sharply defined (corona-type discharges, often erratic, may occur over an uncertain range of still greater pressures) and, for a given system, it is much higher and, therefore, more elusive.

Two opposing effects are responsible for the phenomenon of the critical pressure. First, as pointed out, shorter mean-free paths at elevated pressures impede ionization by collision and so tend to raise the sparkover level. Second, the denser packing of gas molecules renders photoionization more likely and reduces ion diffusion. Thus, pressure facilitates streamer propogation from the anode across the gap and, at the critical pressure, sparkover results.

The likely explanation of the relatively low value attained by the positive sparkover voltage and its concomitant lower critical density is as follows: Intense ionization of the gas is produced in the high-field region in the vicinity of the discharge wire which attracts and removes the highly mobile electrons. The heavy positive ions are repelled from the wire and move slowly toward the collecting electrodes. However, on the far side of the ion cloud (away from the wire), the field, suffering from positive-ion space-charge distortion, is increased and with it, the rate of ionization. Conditions are now favorable for the growth of a positive streamer to develop toward the cathode. On the other hand, when the wire is negative, the positive space charge surrounding it in the corona sheath tends to shield the wire from the anode. This action reduces the field on the anode side and so a higher voltage is needed to promote a spark.

At pressures above the critical value, the slopes of the negative current-voltage curves abruptly and significantly decrease, the discharge is frequently punctuated by irregular sparking as the voltage is raised, maximum currents attainable prior to sustained sparkover are reduced, and the data are less reproducible. Precipitator performance in this postcritical region has never been explored.

Thermal Ionization

We have so far been concerned with mechanisms of ionization stemming from i) electronic and molecular collision processes in the presence of an electric field and ii) photon absorption. At very high temperatures an additional mechanism enters the picture: thermal ionization. This introduces the following new possibilities.

i) Electron-ion production by collision of the gas molecules with each other. Such ionization may occur even in the absence of ionized particles and a high-intensity electric field. It is the high-temperature condition that provides velocities and kinetic energies high enough to cause ionization.

ii) Photoionization resulting from thermal emission of the hot gas. When a high-temperature gas flows through a precipitator, it will emit quanta in accord with the laws of black-body radiations. The electrode surface and the walls of the pressure vessel will reflect most of this radiation. Thus, photons capable of ionizing are always available when the temperature is high enough. Calculation, however, shows that this condition is probably not met under present circumstances.

iii) Ionization by collision with high-energy electrons that have been generated by the above two processes.

Apprehensions arise in running precipitators at very high temperatures because significant thermal-ionization rates may lead to catastrophic currents at reduced voltages. Earlier predictions that this condition might occur at a temperature of about 1100 K (6) have been shown experimentally to be untenable (3). Revised theoretical work (8) now suggests that whereas thermal effects may become noticeable below 1100 K, practical high-temperature precipitation may be limited only by temperatures exceeding 1400-1600 K. The lower limit of this range would apply to gases containing a component of low ionization potential, say potassium, in quantities as low as one atom in 10^4. Potassium is singled out because of the alkali metals (all of which have characteristically low ionization potentials), it is the most common, constituting 1.4 percent of the earth's crust. Hence, the probability of its appearance in industrial gases is not remote.

It is worthwhile bearing in mind, however, that normally unanticipated minority ionic species may effect the corona process. According to Loeb (15), the relatively high negative currents and low accompanying sparkover voltages that several observers have reported at high temperatures (27, 33, 36) are probably due to the action of the O^- or O_2^- ion. The point to consider is the fraction of the time an electron can remain detached from a molecule or atom, the average detachment interval increasing with temperature. Since the negatively ionized oxygen molecule O_2^- sheds its electron at about 600 K, followed at somewhat higher temperatures by the O^- ion, the high temperatures of present interest should be dominated by heavy free-electron concentrations. This condition gives rise to heavy currents and causes a loss of corona stabilization otherwise resulting from negative-ion space charge. In Loeb's view, the O^- ion with an electron affinity of 1.5 eV, well below the 4.3 eV ionization potential of potassium, would

probably be the primary culprit for the ultimate high-temperature failure of the precipitation process in oxygen-bearing gases. However, if potassium were present in sufficient quantity, its effect would govern.

It must be emphasized that details of the thermal-ionization process described above are, as applied to precipitators (even under laboratory conditions), largely hypothetical. For example, none of the ionic species has been positively identified in a high-temperature precipitator test, and the predictions of limiting temperature are not supported in any consistent manner by the experimental data.

Earlier Studies

Previous investigations relating to this study are cited, as appropriate, in the text. Other precipitation work worthy of note is that of Koller and Fremont, dust-free, in air and methyl chloride, to 800 K and 500 kPa (14); Thomas and Wong, dust-free, in air, to 1100 K and 810 kPa (33); Shale and associates, with and without dust, in air and flue gas, to 1100 K and 650 kPa (25-32); and most recently, Brown and Walker, with dust, in flue gas, to 1200 K and 896 kPa (3).

SECTION 2

CONCLUSIONS

At high temperatures and pressures such as are found in advanced coal-conversion processes, electrostatic precipitators exhibit potentially higher collecting efficiencies than prevail under conventional conditions of precipitator application. High efficiencies are an anticipated consequence of the increased voltages that can be applied to the precipitator for a broad range of pressure-temperature combinations. This efficiency effect is unique for precipitation; in other particulate collection methods, efficiency generally decreases with increasing temperature and pressure.

In the present study, no practical upper limit is reached for electrostatic precipitation at temperatures and pressures as high as 1360 K and 3550 kPa. In some instances, however, limits imposed by the critical pressure are approached. The critical pressure is the lowest elevated pressure at which corona-starting and sparkover voltages coincide.

Increasing the temperature raises the critical pressure and so results in a broader operating range of pressure. The negative-corona critical pressure, attained here only at room temperature, is found to be significantly higher than the corresponding positive value. Positive-corona critical pressure, reached at all temperatures, is observed to increase with decreasing wire diameter.

The higher the pressure, the more slowly does current increase with voltage, i.e., the more stable the discharge. As a practical rule, high pressure should accompany high temperature.

Positive sparkover voltage exceeds negative for conditions of low gas density and high temperature. For high density, negative sparkover voltage is higher than positive.

On the basis of the stable corona currents obtained for the three gas compositions examined -- air, combustion gas and a substitute fuel gas -- electrostatic precipitation is judged feasible in each case. The fuel gas yields the highest corona currents for a given voltage.

The amplitude of discharge-electrode oscillations is dependent on electrode length, shape, tension and material. Short, rigid or highly stressed electrodes produce minimal oscillation. The rigors of high-temperature service require discharge and collecting electrodes of high tensile strength and high oxidation and carburization resistance. Oxidation and carburization result in an expanding scale growth that alters the electrode surface and affects both corona-starting and sparkover voltages. Inconel 601 performs satisfactorily at temperatures up to 1360 K.

SECTION 3

RECOMMENDATIONS

In view of the encouraging results obtained so far but which are limited to a particle-free system it is recommended that we next proceed to the design and operation of a pilot precipitator treating fluidized-bed combustor or gasifier effluents. Estimates of particle-migration velocity derived from the current-voltage data of this report make possible the rational design of an operational precipitator. Pilot tests with such a precipitator will reveal the effect of the presence of particulates on electrical performance, will permit the checking of predicted values of particle-migration velocity, and will provide experience in aerosol sampling and precipitate removal under extreme conditions of temperature and pressure.

The diameter of the pilot collecting electrode will be severalfold greater than in the present case. Beneficial consequences of the larger electrode include a more stable corona characteristic and higher critical pressure.

High-temperature evaluation of materials of construction, with special attention to electrodes and insulators, will extend into the pilot phase.

SECTION 4

EXPERIMENTAL APPARATUS AND PROCEDURE

TEST PRECIPITATOR

The experimental electrostatic precipitator comprises a concentric wire-pipe electrode system surrounded by an electric heater. The entire assembly is enclosed in a pressure vessel as shown in Figure 1. The vessel, designed to withstand pressures upwards of 3550 kPa, is assembled in three sections. Mounted on the uppermost part is an alumina bushing through which a high-potential conductor enters the vessel and connects to the discharge electrode. A rupture disc in the top flange protects against the hazard of overpressurization. The bottom third of the vessel has a side access port for making adjustments and observations, a support insulator for centering the lower end of the discharge electrode, and a gas inlet. The precipitator tube together with a three-zone heater is fixed in the center segment of the pressure vessel. Disc-shaped alumina end pieces serve to center the precipitator tube at its top and bottom, and by restricting convection currents, help maintain a more uniform temperature over the tube length. The heater is packed in a layer of Kaowool insulation about 5-cm thick; this material fills the space between the heater and the wall of the pressure vessel.

The tubular (collecting) electrode is fabricated from Inconel 601 and is 7.26 cm in internal diameter.

In order to obtain a corona-current measurement uninfluenced by end effects, the 76.2-cm long collecting electrode is divided into three tubular segments, each electrically insulated from its nearest neighbor(s). The 61.9-cm long midsection is grounded through a current measuring device --either a milliammeter or one axis of an X-Y recorder. In this manner, only current to the midsection is measured. The terminal guard sections, each 7.15-cm long are grounded directly, and currents to them are excluded from the experiment. The ends of the guard sections are flared sufficiently outward to insure that sparkover occurs not at the edges of the tube but in its long straight portion.

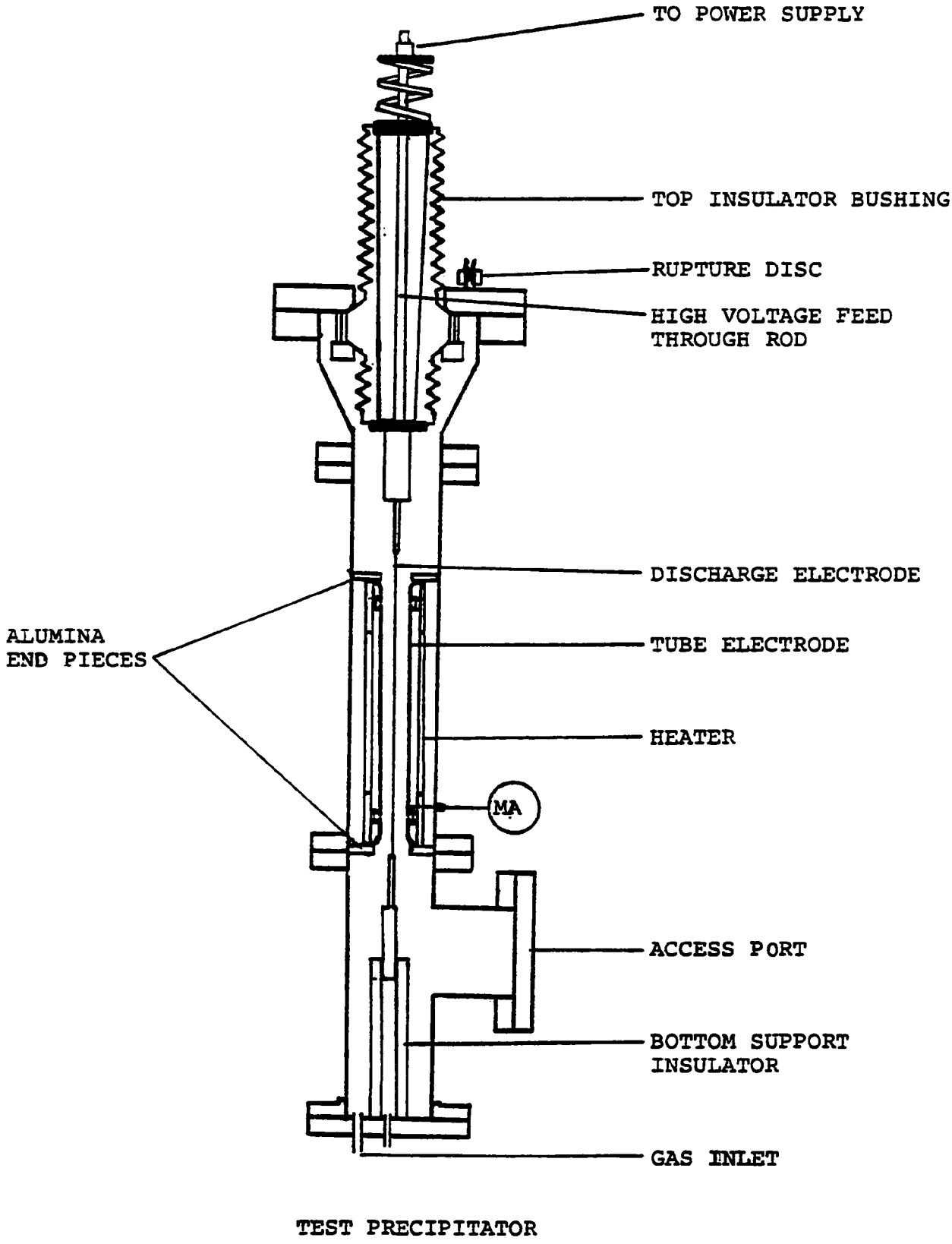

Figure 1. Laboratory Precipitator and Pressure Vessel for Test Program

The wire discharge electrode, also of Inconel 601, is secured at its upper end, via a shroud, to the high-voltage feedthrough rod. At its lower end, the wire is connected, again by means of a shroud, to a 0.98-kg weight. The weight keeps the wire taut and suppresses oscillations. Three wire diameters are employed in these tests: 1.575 mm, 2.344 mm and 3.175 mm.

HIGH-VOLTAGE POWER SUPPLY

The high voltage power supply is a silicon-rectified voltage quadrupler (Figure 2a) on the secondary output of a 105-kV peak transformer, yielding voltages to 400 kV peak and currents to 60 mA. The transformer primary voltage is controlled by twelve variable transformers driven by a variable-speed motor. The power-supply output is connected to the experimental precipitator through a series resistance of 145,000 ohms and an inductance of 0.57 mH to protect against spark transients. Output-voltage ripple at maximum precipitator current is less than one percent of the rms voltage and is, therefore, assumed negligible.

High voltage is measured by means of the resistive divider network shown in Figure 2c. The voltage is read both on a voltmeter and the remaining axis of the X-Y recorder mentioned previously. Thus, provision exists for the automatic plotting of corona current as a function of applied voltage. The high-voltage measuring circuit is calibrated in terms of the accurately measured currents flowing through the precision resistors of the divider and, independently, by an electrostatic voltmeter.

The current arm of the recorder is protected from transient surges by a needle spark gap, an inductor, a metal-oxide varistor, and shunt capacitors (Figure 2d).

Polarity may be changed by reversing the silicon rectifiers.

TEMPERATURE CONTROL SYSTEM

The temperature of the gas and the precipitator is controlled by a three-zone heater surrounding the tube. The top and bottom zones, each 15.2 cm long, control the temperatures at eachend of the tube. The end heaters, in combination with the 45.7-cm long center zone, maintain a uniform temperature along the entire tube length. Three proportional controllers employing thermocouples placed next to the heater elements maintain a set temperature level using the control circuit shown in Figure 3. For additional protection from high-voltage transients, each heater is grounded inside the pressure vessel, with one power lead emerging from each zone element. An isolation transformer applies voltage to each variable transformer and heater through the relays controlled by the outputs of the proportional controllers.

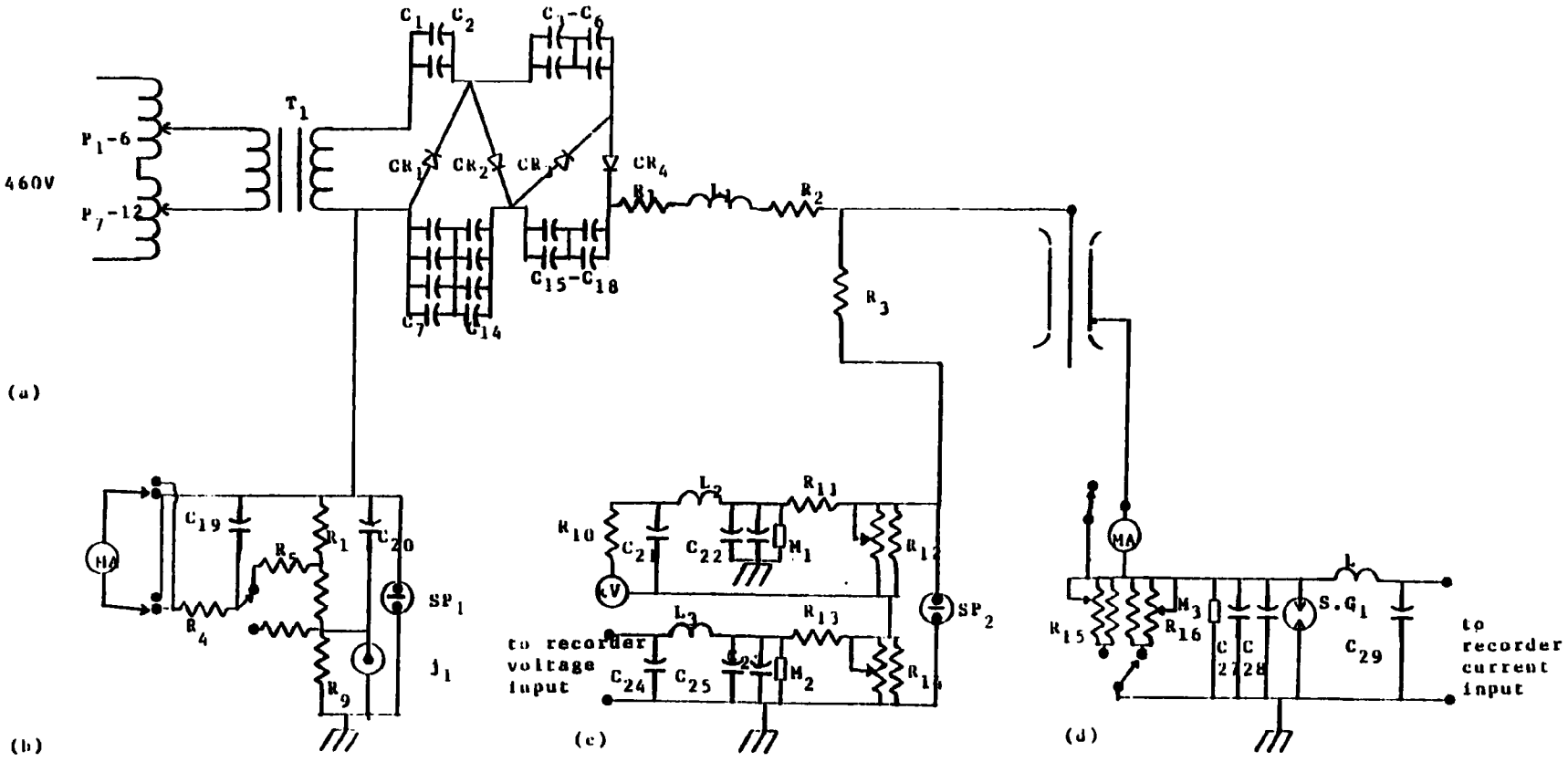

Figure 2 Power Supply and Instrumentation Measuring Circuits:
(a) Power Supply Quadrupler
(b) Total Current Circuit
(c) Voltage Divider Circuit
(d) Tube Current Circuit

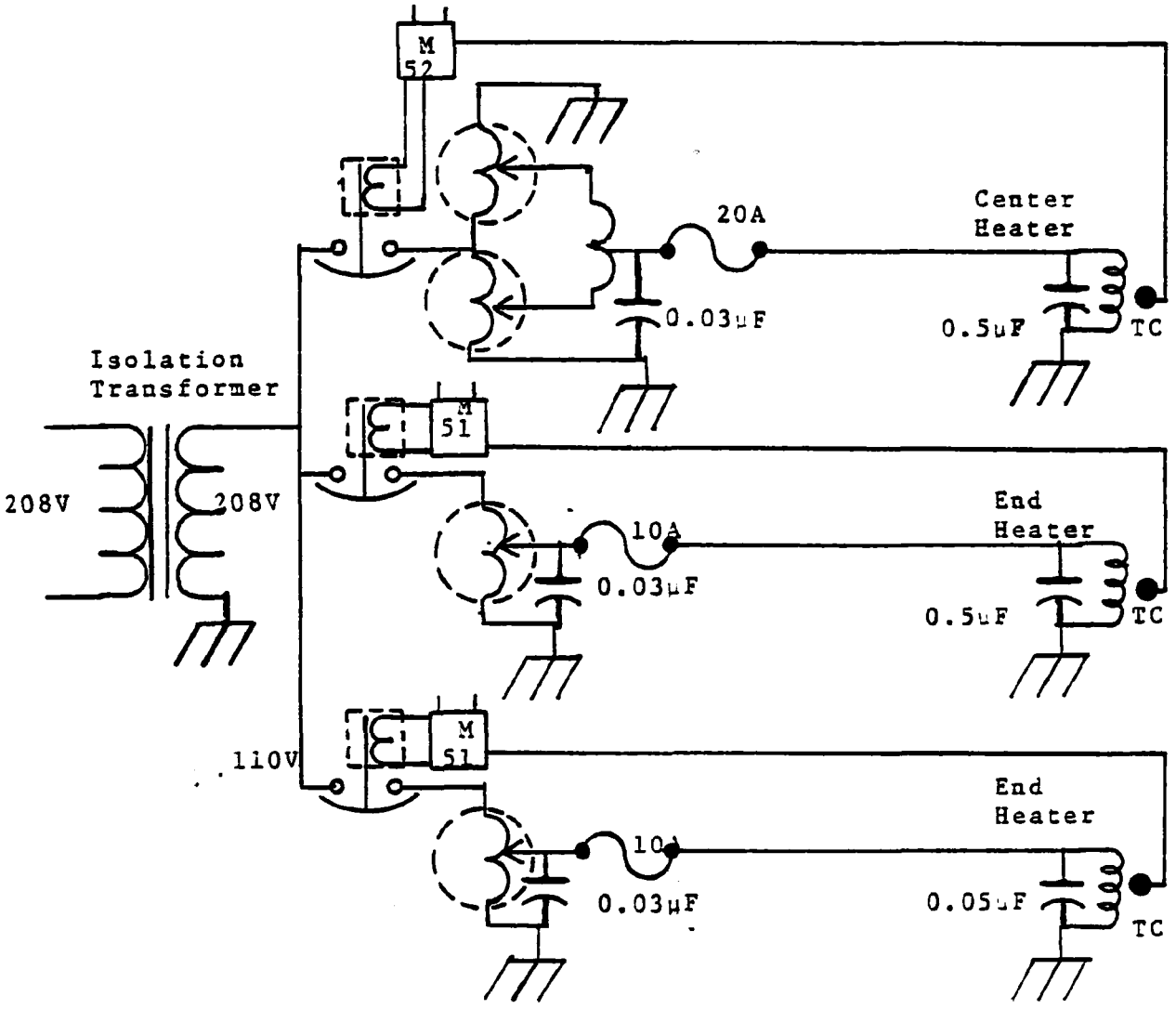

HEATER CONTROL CIRCUIT

Figure 3. Three-zone Precipitator Heater and Control Systems for Temperatures to 1400 K.

The temperatures of the interior of the tube is calibrated against the temperature of the thermocouples located at the heating elements. This is done by recording temperatures at six positions along the inner length of the tube for each controller setting. The results form the temperature-calibration curve shown in Figure 4. Using this calibration curve with the three-zone control, a uniform temperature can be established and held throughout the entire tube for each test.

GAS-FLOW SYSTEM

The gas flow system is designed to control the final gas composition within the precipitator. The process flow system, shown in Figure 5, has (1) five individual gas cylinders, with regulators containing N_2, He, dry air, and mixtures of N_2 - CO_2 and CO_2 - O_2; (2) a set of four pressure guages appropriately spanning the required pressure range to 6890 kPa; (3) provision for passage either through or around the humidifier; and (4) heated lines into the precipitator vessel. Sampling points are available for analysis of the gas.

The humififier as shown in Figure 6 is required for adding moisture to the gas mixture. By dispersing the gas through a heated water bath, the gas becomes saturated at the bath temperature. The gas is then immediately heated to a higher temperature (477 K) in a heated packed bed and sent through heated lines to the pressure vessel, constantly maintaining the gas above its dew point. A water-bath temperature of 388 K will put 5 percent water vapor into the gas phase with a total pressure of 3550 kPa. The test facility (Figure 7) is arranged to provide maximum control and safety during the test runs.

Three gas compositions were used for testing: air, a simulated combustion gas, and a substitute fuel gas with component concentrations shown in Table 1.

Table 1

TEST GAS COMPOSITIONS

(Volume %)

Component	Fuel Gas Mixture	Combustion Gas Mixture	Air
CO_2	23.0	9.2	-
He	18.5	-	-
O_2	-	2.8	21
N_2	53.5	83.0	79
H_2O	5.0	5.0	-

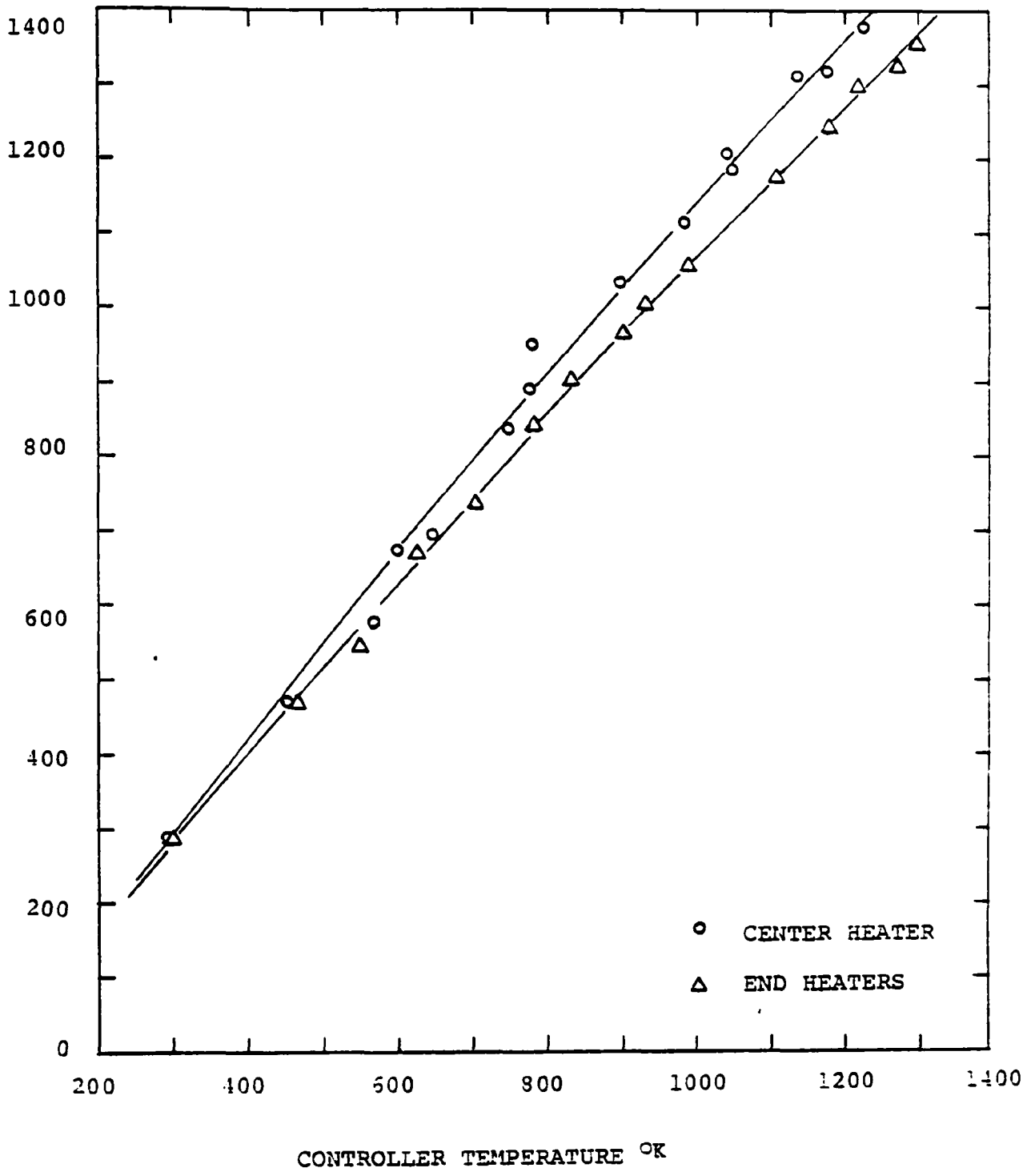

Figure 4. Precipitator Tube and Internal Gas Temperature Based on Each Heater Thermocouple Temperature.

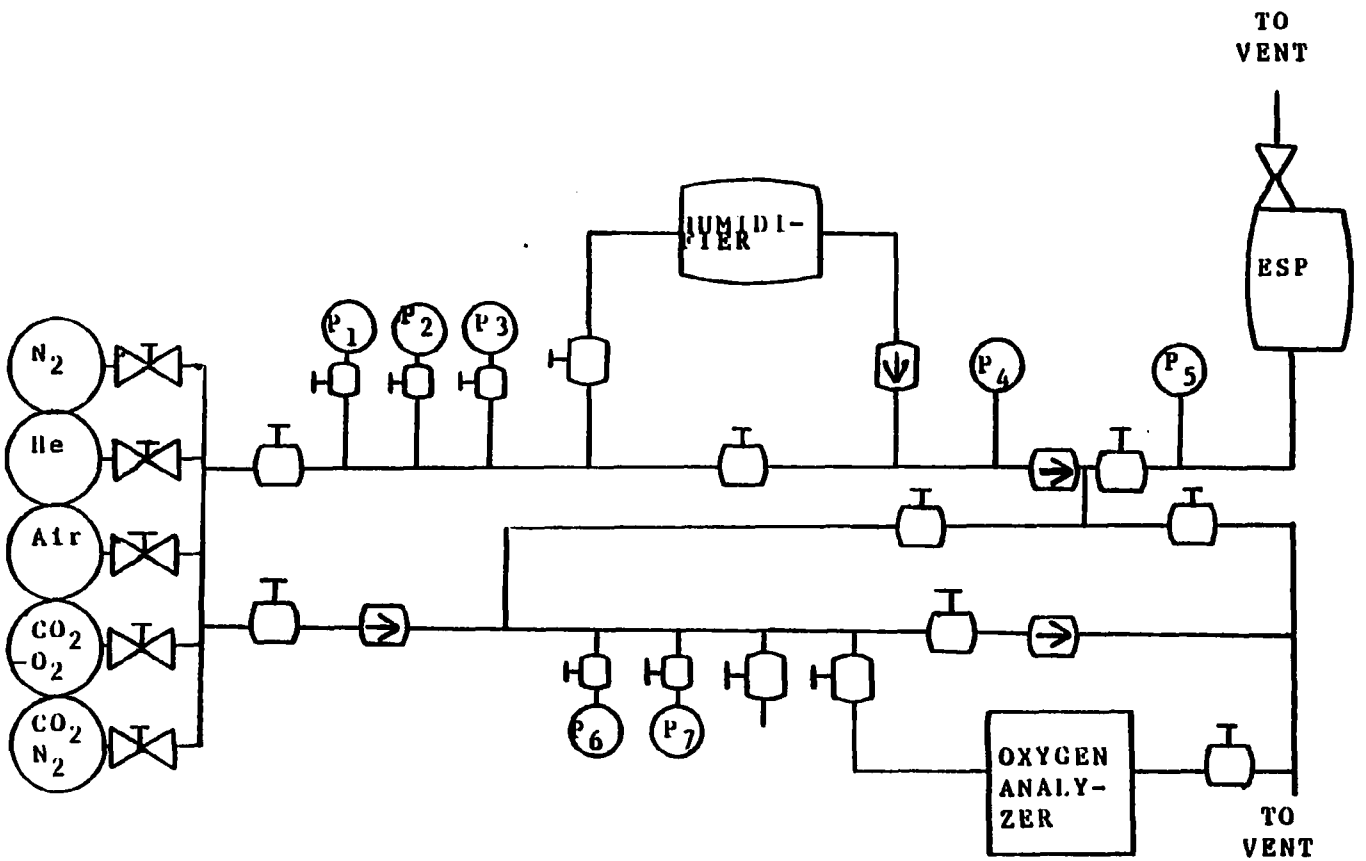

PRESSURIZING FLOW SYSTEM

Figure 5. Gas Pressurizing and Mixing Flow System Used to Fill Precipitator for Each Test Series.

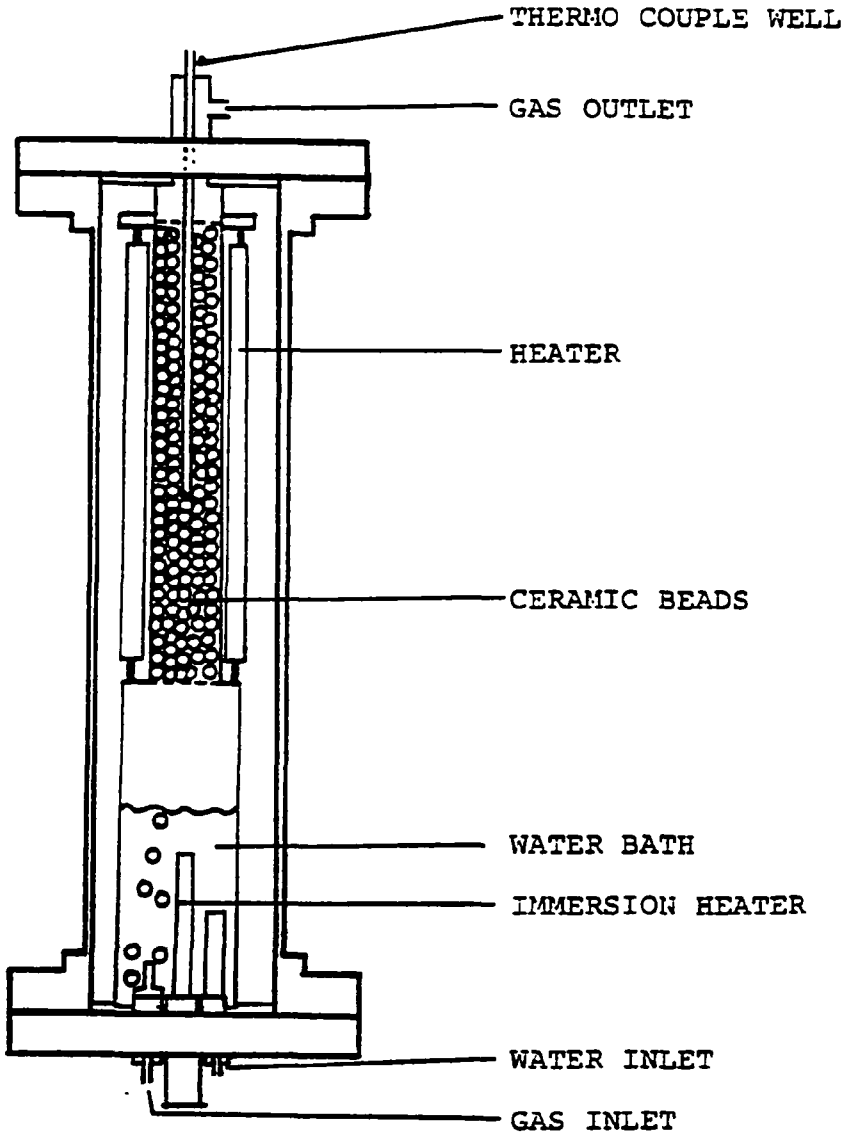

HUMIDIFIER

Figure 6. Internal Schematic of Humidifying System Showing Water Bath and Heater Used for Gas Saturation and Moisture Level Control.

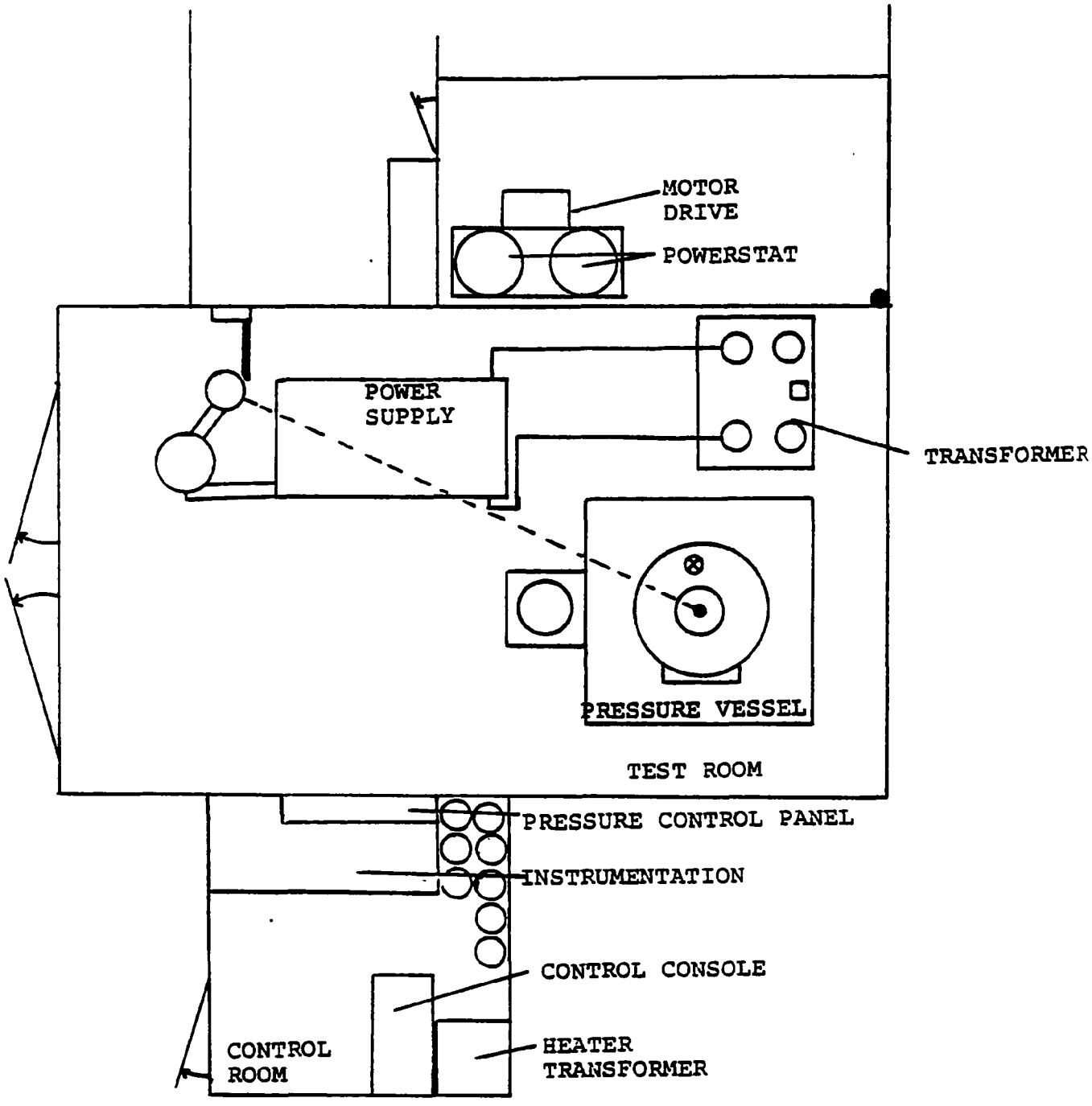

EQUIPMENT FLOOR LAYOUT

Figure 7. Schematic Layout of all Test Equipment, Power Supply and Instrumentation Showing Both the Test Room and Control Room.

Dry compressed air (dew point, 216 K) is used for all air tests. The humidifier is bypassed when pressurizing the vessel to 3550 kPa with air.

To simulate combustion gas, after purging the pressure vessel with nitrogen, the gas components are passed through the humidifier in the following manner:

(1) Using a 77%-CO_2 and 23%-O_2 mixture, the pressure vessel is filled to 550 kPa.

(2) Using 99.99% N_2 gas, the pressure vessel is filled from 550 kPa to a final pressure of 3550 kPa, yielding the composition given in Table 2.

The substitute fuel gas is prepared in a similar fashion, by passing all gases through the humidifier:

(1) Using a 30%-CO_2 and 70%-N_2 mixture, the precipitator is pressurized to 1140 kPa.

(2) Using pure helium, the vessel is filled from 1140 kPa to 1830 kPa.

(3) The final step is to finish filling the pressure vessel to 3550 kPa with the 30%-CO_2 and 70%-N_2 mixtures. This results in the composition shown in Table 2.

Helium is chosen as a substitute for the hydrogen of actual fuel gas because the two constituent gases offer the closest readily attainable match of thermal conductivity and ion mobility. Carbon monoxide is replaced with carbon dioxide. A comparison of conductivity and mobility values for the various gas mixtures is shown in Table 2. Calculation procedures are found in Appendices A and B.

Table 2

THERMAL CONDUCTIVITIES AND IONIC MOBILITIES OF GAS MIXTURE

	k (mW/m-K)	b_o^- ($cm^2/(s\text{-}V)$)	b_o^+ ($cm^2/(s\text{-}V)$)
Real Fuel Gas	38.3	1.64	1.49
Substitute Fuel Gas	41.1	1.87	1.58
Combustion Gas	28.4	1.91	1.59
Air	29.9	2.5	1.8

TEST CONDITIONS AND PROCEDURE

The experimental procedure is chosen (1) to meet the rigors of extended high-temperature and high-pressure testing, (2) to obtain sufficient data to estabish ranges of corona stability, and (3) to show effects of composition, electrode geometry, and polarity. The ranges for each variable are shown in Table 3.

Table 3

EXPERIMENTAL VARIABLES

Temperature	294, 533, 811, 1089, 1366 K
Pressure	101 to 3550 kPa
Wire Diameter	1.575 mm, 2.344 mm, 3.175 mm
Polarity	positive, negative
Gas Mixture	air, combustion gas, substitute fuel gas

Three wire sizes are used in the air tests; however, only one wire size is used for the combustion-gas tests and the substitute-fuel tests.

In conducting the tests, a steady-state temperature is attained by maintaining the heaters at the desired temperature setting for a minimum period of ten hours, with the gas mixture added four hours prior to testing.

In moving from one condition of pressure to another, but at constant temperature, the gas is always released from the vessel in order to retain constant composition and thermal stability. At each pressure, results for both negative and positive wire polarity are obtained.

Prior to recording a current-vs-voltage curve, the voltage is held at sparkover for a period of two minutes to "condition" the electrodes. Duplicate curves are then recorded with both increasing and decreasing voltage. The minimum voltage at which repetitive sparking occurs over a 2-min interval is reported as the sparkover value. Corona-starting voltages are determined by two methods: (1) observation of voltage at which corona pips disappear on an oscilliscope with decreasing applied voltage and (2) extrapolating the current-voltage curve to zero current. Sometimes, a sharp elbow occurs at currents of a few tenths of a milliampere per meter or less. See, e.g., Figure 13e. In such a case, the knee is disregarded in extrapolating the curve.

In the presence of corona, the gas pressure within the vessel increases. Changes of as much as 3 or 4 percent, corresponding to temperature increases of 5 or 6 percent, are observed under some conditions. Gas density, however, remains essentially constant (± 2 percent).

DISCHARGE-ELECTRODE OSCILLATION TEST

Different discharge electrode geometries are evaluated at elevated wire temperatures to determine the effect of geometry on (1) amplitude of oscillation and (2) strength of material. Previous experience shows that wire oscillations result in substantially lower sparking voltages due to reduced clearances. The equipment designed to test the several geometries is shown in Figure 8. A collecting pipe electrode made of type 316 stainless steel with an internal diameter of 0.213 m and an overall length of 3.658 m is securely mounted on a support structure that isolates it electrically from ground. The discharge electrode is centrally mounted within the pipe, and a weight is attached to the bottom end. This tensioning weight is needed to keep the wire taut and dampen potential oscillations. A stepdown transformer, connected to each end of the wire electrode, provides the current needed to reach the high electrode temperatures approaching 1366 K. A mirror and graduated scale are placed beneath the pipe to permit the oscillations to be observed and measured. A 106-kV peak, high-voltage, reversible-polarity power supply is connected to the pipe. Current- and voltage-measuring circuits are shown in Figure 8.

Electrode temperature is determined by using temperature-sensitive color indicators on each electrode. The various geometries of the electrodes are shown in Figure 9 and are tabulated below:

Table 4

ELECTRODE GEOMETRIES

	7.94 mm	Twisted Square
	6.35 mm	Twisted Square
	6.35 mm	Round Wire
	6.35 mm	Stranded Cable
three	2.77 mm	Twisted Wire
	2.77 mm	Round Wire
two	1.59 mm	Barbed Wire with 19-mm Barb Diameters

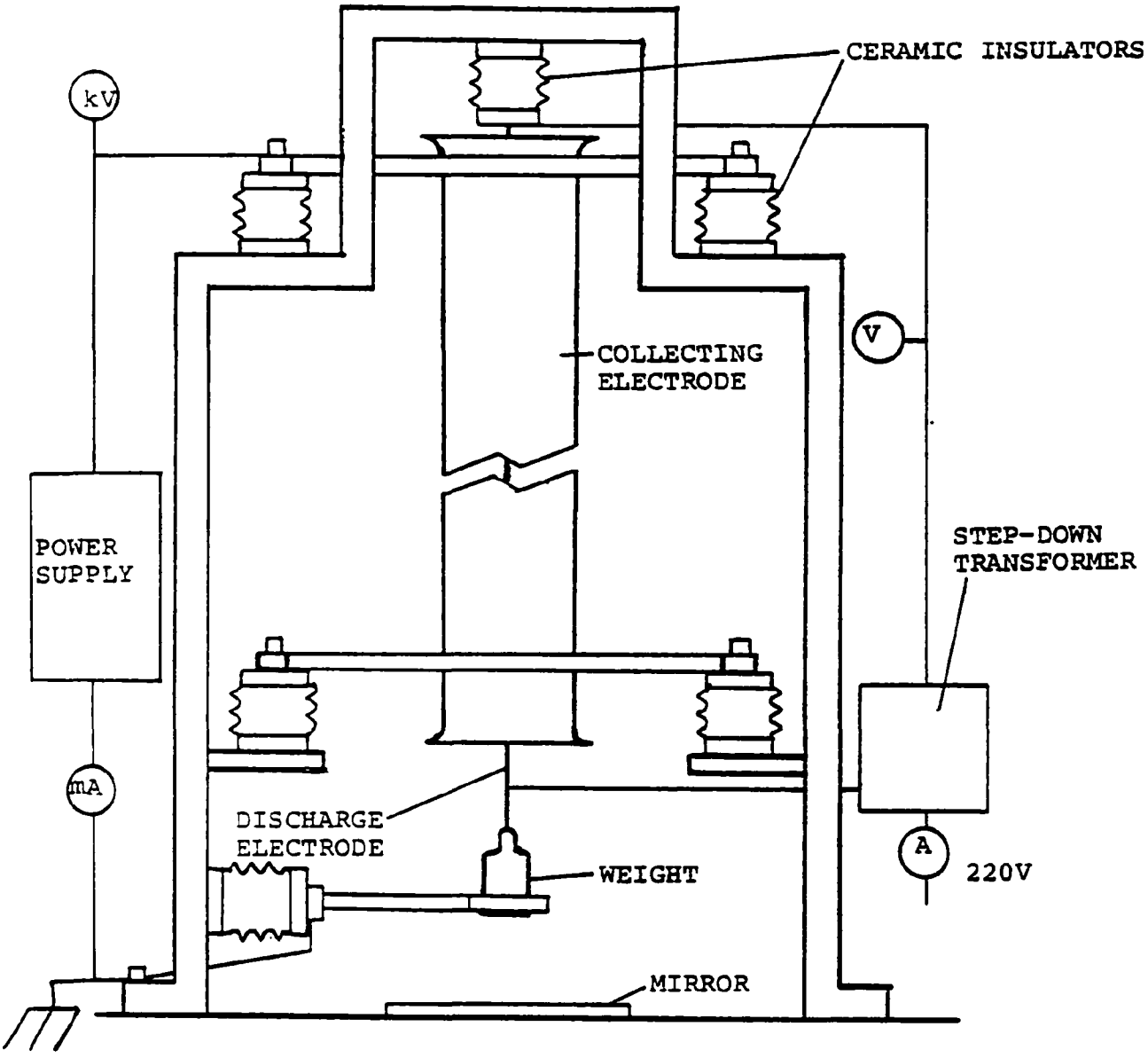

OSCILLATION TEST

APPARATUS

Figure 8. Laboratory Apparatus Set to Test Effect of Electrode Size and Geometry on Degree of Oscillation at High Voltage.

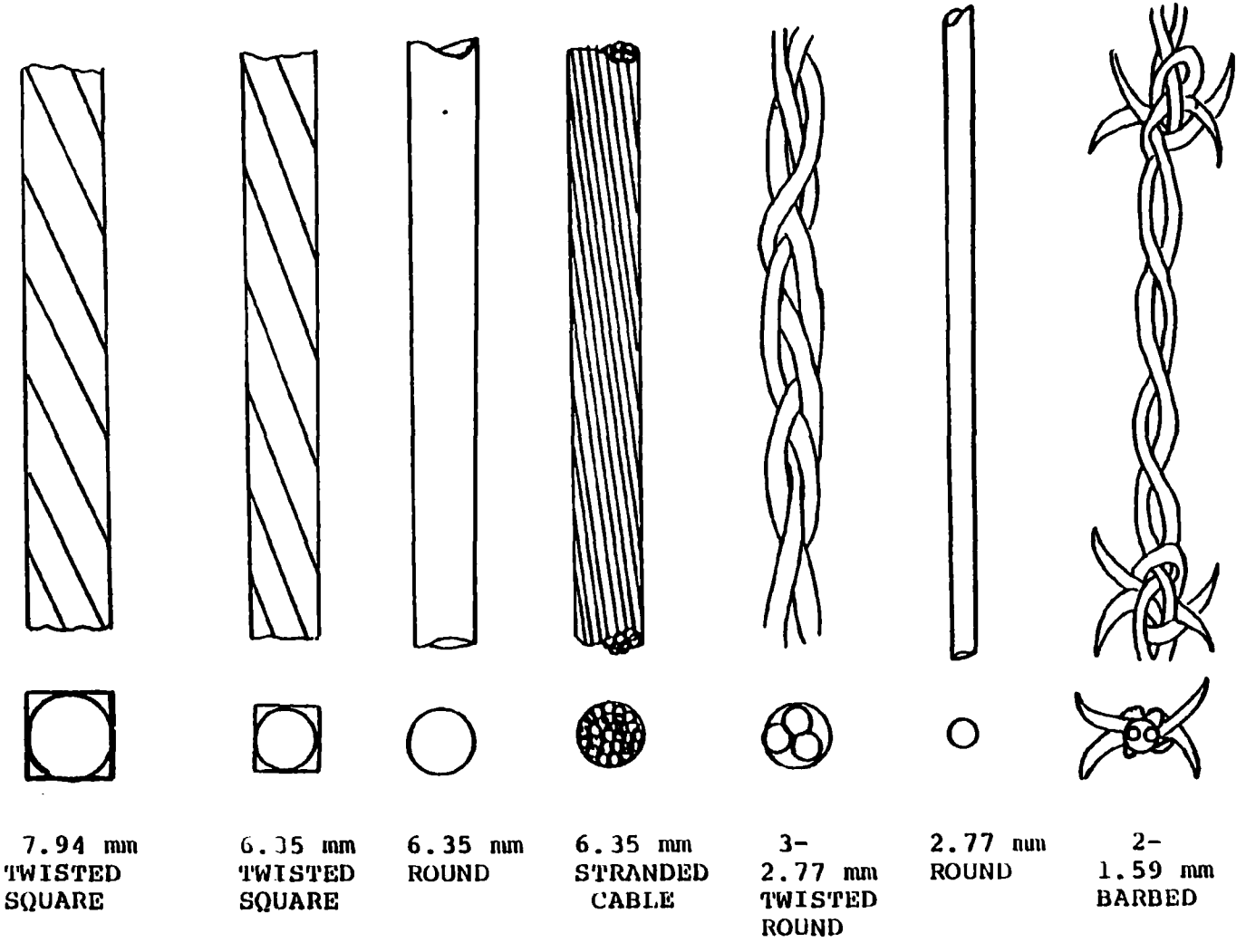

Figure 9. Cross Sectional and Lateral Views of the Seven Electrode Geometries Used in the Oscillation Study.

SECTION 5

RESULTS AND DISCUSSION

THE EXPERIMENTAL DATA

The raw experimental data, consisting of curves of linear current density (mA/m) vs impressed voltage (kV) are reproduced in Figures 10 through 13 for air, Figure 14 for simulated combustion gas and Figure 15 for substitute (i.e., noncombustible) fuel gas. Corona-starting and sparkover voltages, derived from these curves and independent measurements, are shown as functions of relative gas density δ in Figures 16 to 18 for air, Figure 19 for combustion gas, and Figure 20 for substitute fuel gas. Figures 21 and 22 compare experimental and calculated corona-starting fields.

The relative gas density δ is taken with respect to atmospheric pressure (P_o = 101.3 kPa) and room temperature (T_o = 294 K)

$$\delta = \frac{T_o}{P_o} \frac{P}{T} = 2.90 \times 10^{-3} \frac{P}{T}. \qquad (1)$$

In Figures 10 through 15, all current-voltage curves terminate in sustained sparkover indicated by a short broken line segment.

TEMPERATURE/PRESSURE LIMITATIONS ON CORONA STABILITY

General Remarks

Our first and most important objective is to examine the data for the purpose of establishing temperature or pressure limits to a stable corona discharge. Such limits may be either of a fundamental nature, that is, inherent in the physics of the gaseous discharge, or practical, as for example, restrictions imposed by the strength of materials at high temperature. Focussing for the present on the fundamentals, we search the current-voltage curves of Figures 10 to 15 for i) excessive currents at low voltages resulting from thermal ionization (where "excessive" and "low" are taken from the point of view

of practical precipitator operation) and ii) the disappearance of (stable) corona due to the manifestation of the critical pressure.

Excessive Current

Catastrophic high-temperature currents are not observed in this study under any conditions. This significant point is evident over the full range of experimental pressures (atmospheric to 3550 kPa) and temperatures (294 K to 1366 K) and both polarities.

It might be expected that runaway currents at low voltages are most likely to occur at the lowest gas densities. We note, however, for the negative corona at δ less than about unity, the reverse is generally true: the presparkover currents are much less than at higher densities. The curves of Figures 12(d), (e) and (f) for $\delta = 0.33$ and 0.34 are typical examples. For positive polarity, the low-δ presparkover currents are mixed: in most cases they are not lower than at higher δ. Still considering the positive discharge, we see that combustion gas (Figure 14), and fuel gas to a lesser extent (Figure 15), but not air, reveal a tendency to sparkover without corona at the lowest densities. But, in any event, a problem of high gas conductivity associated with low densities does not arise.

Reduced presparkover currents at low δ have been reported elsewhere for both polarities in air and are not a consequence of high temperature (20).

CONCLUSION: Uncontrollable corona currents, whether due to high temperature or low density, do not occur in these tests.

Positive Critical Pressure

On the basis of earlier critical-pressure studies (20, 21) it might be supposed, at least at lower temperatures, that the critical-pressure phenomenon would set an upper-pressure limit to the positive corona in the present experiments. That this is indeed the case is borne out by the positive current-voltage curves of Figures 10 to 13 for air, Figure 14 for flue gas, Figure 15 for combustion gas, and the associated voltage-density curves of Figures 16 to 20. It is also seen from the curves --upon converting density to pressure -- that the positive critical pressure increases with temperature. This comes about because the greater molecular diffusivity prevailing at the higher temperatures more effectively suppresses the sparkover streamer before it completely bridges the interelectrode space (12). The effect described has not hitherto been demonstrated over so wide a span of temperatures.

CONCLUSION: Temperature raises the positive critical pressure.

Negative Critical Pressure

The negative critical pressure, as already explained, should be sought at higher levels than the positive, all other conditions being held fixed. The critical pressure, it is seen, is attained, or at least closely approached, for the positive corona in every case (Figures 10-15). The negative current-voltage curves of Figures 10 to 15 suggest, especially at the lower temperatures, that the critical pressure is being approached - in Figure 10(d) perhaps even attained --as the pressure nears its experimental maximum. I.e., with increasing pressure, sparkover voltages increase less rapidly or actually drop, and maximum presparkover currents fall abruptly. Since the negative-corona data permit a lower bound to be set to any negative critical pressure, it is clear, by comparison of families of curves for each polarity, that the negative critical pressure exceeds the positive. It is further apparent that the negative critical pressure, like the positive, increases with temperature. In other words, the higher the temperature, the greater the range of pressures of the negative corona. The highest temperatures of this study, instead of rendering the corona unstable by reason of thermal ionization, actually enhance corona stability by moving the critical pressure outside the pressure range of interest.

CONCLUSION: The negative critical pressure exceeds the positive.

CONCLUSION: Temperature raises the negative critical pressure.

Practical Precipitator-Tube Diameter

The diameter of the outer electrode used in this study is 7.62 cm, about one-third of the diameter likely to be selected in a practical precipitator. Since the negative critical pressure for wire-tube configuration in air is proportional to the tube diameter (20) a realistic practical tube diameter of three times that used here should eliminate the critical-density restriction even at the lowest temperatures employed.

Another matter for concern are the steeply rising currents typifying most of the current-voltage curves, and especially those for negative corona in substitute fuel (Figure 15(f), (g), and (h). In these cases, rough extrapolation to a threefold greater tube diameter may be made by means of the quadratic corona approximation

$$j = \frac{8\pi\varepsilon_o b}{r_o^2 \ln (r_o/r_i)} V(V-V_c)$$

where:

j is current density (A/m)

ε_o is permittivity of free space (8.85×10^{-12} F/m)

b is ion mobility (m^2/sec-v)

r_o is tube radius (m)

r_i is wire radius (m)

V is applied voltage (V)

V_c is corona-starting voltage (V)

It is clear that a threefold increase in r_o will reduce j by about an order of magnitude at a given voltage. The slopes of the current-voltage curves will be much shallower, and the currents correspondingly more susceptible to control.

CONCLUSION: No pressure limitations to negative-corona stability over the range explored are expected in a precipitator tube of practical diameter.

The effect of temperature in reducing gas density or causing thermal ionization tends to raise the current. Pressure, on the other hand, compensates by reducing current.

CONCLUSION: Generally speaking, high pressure should accompany high temperature as long as the critical pressure is not too closely approached.

POLARITY EFFECTS

Background Considerations

It is virtually axiomatic in conventional precipitation engineering, and has been since its early recognition by Cottrell, that the negative corona yields higher sparkover voltages than the positive and, consequently, higher collecting efficiencies. The negative advantage, however, is demonstrably not universal. Sometimes, at least when the electrodes are clean, there is little apparent difference between the polarities (20), and sometimes, as for certain combinations of high-resistivity precipitate and pressure, the positive sparkover voltage may exceed the negative by many tens of kilovolts (22). Additional actual and theoretical cases are cited by Cooperman (7, 9).

The foregoing higher positive sparkover voltages apply at room temperature. At elevated temperatures, several investigators (27, 33, 36) have also reported higher positive sparkover voltages, but here the high-temperature condition is an essential feature of the phenomenon. In the high-temperature negative corona, the equilibrium attachment-detachment conditions that seem to obtain give rise to heavier free-electron concentration Two things now happen that superimpose their effects, in some degree, on the usual corona processes. The high-mobility free electrons are rapidly swept out of the interelectrode gap by the field, an action that yields higher negative than positive corona currents at a given voltage. In addition, the resultant loss of negative-ion space charge will fail to provide for stabilization of the negative discharge by suitable space-charge modification of the interelectrode field as is normally the case at ordinary temperatures. Negative-corona sparkover, therefore, occurs at lower levels than positive.

Experimental observations in Air

Comparison of the sparkover-voltage vs gas-density data of Figures 16-18 reveals a tendency for the positive sparkover voltage to exceed the negative at temperatures of 533 K and higher and for air densities δ less than about 1 or 2. Now the data are not unequivical on this score in each case, a not unusual development in view of the uncertainties of the measurements. The trend, nevertheless, seems clear, particularly when supported by experimental results of earlier workers. The significantly higher negative than positive currents prevailing at a given voltage at the higher temperatures are, however, unmistakable (Figures 10-15).

The somewhat higher negative than positive currents that may be observed at the lower temperatures are, in part, to be attributed to the significant free-electron component of the current present for relatively long mean free paths (low δ) and narrow interelectrode spacing.

Again, it may be generally (though not invariably) seen from Figures 16-18 that, above an air density of 1 or 2, the negative sparkover voltage is higher than the positive. Since increased density reduces the mean free paths and mobilities of the charge carriers, enhanced electron attachment an increased negative-ion space-charge density might be expected to lead to higher negative sparkover voltages. That is, high pressure in combination with high temperature restores, in a sense, the low-temperature situation.

Experimental Observations in Combustion and Fuel Gases

In the case of substitute fuel gas (Figure 20) the positive sparkover voltage exceeds the negative, over the full temperature range shown, up to a density of 6 or 7. For combustion gas (Figure 19) the transition occurs at about a density of 4 for temperatures of, or greater than, 1089 K.

CONCLUSIONS: At a given density and voltage, the negative corona current exceeds positive, the difference increasing with temperature.

CONCLUSION: High pressure favors higher negative sparkover and low pressure higher positive sparkover.

CORONA-STARTING VOLTAGE

Data Fluctuations

Each frame of the corona-starting voltage vs gas-density data (Figures 16-20) consists of a series of corona-starting measurements taken at a fixed temperature, with descending pressures, over relatively brief intervals of time. Longer-term fluctuations of the data, caused by temperature cycling and other factors, are not expecially apparent in any single frame. Such fluctuations in corona starting voltage measurements do, nevertheless, exist, expecially for the negative corona (19). Since, in this study, thermal ionization is not primarily responsible for the discharge in the negative corona, it is the wire itself, rather than the gas, that is the source of secondary electrons needed to maintain the current. Emission from the wire is dependent on the physical and chemical microstructure of its surface, the presence of oxides and other films, and similar influences not amenable to experimental control. Surface contaminations and irregularities produce electrical effects that are intensified by the diminution of lateral diffusion at high gas densities, with a subsequent increase in space-charge distortion.

The situation is much different in the positive corona. Here the cathode is in a reduced-field zone and cannot contribute significantly to the maintenance of the discharge. The source of required seondary electrons -- again assuming minimal thermal ionization effects -- is the gas surrounding the anode wire. Since the corona-starting voltage is now relatively unaffected by the status of the elctrode surface, it is less likely to fluctuate with time or temperature.

Irregularities in the corona-starting voltage may influence the shape of the current-voltage curve well removed from the point of corona onset. This behavior can account for much of the nonreproducibility exhibited by the experimental results.

Peek's Equation

A quantitative idea of the experimental variability of the corona-starting voltage is conveniently obtained by comparing measured corona-starting fields at the wire surface and comparing them with values calculated from the Peek relationship (17)

$$E_c = m \{ A\delta + B(\delta/r_i)^{\frac{1}{2}} \} \quad (3)$$

where:

E_c is corona starting field (V/m)

m is surface roughness factor (ds)

δ is relative gas density (ds)

r_i is wire diameter (m)

For air, recommended values of the constants A and B are 32.2 x 10^5 V/m and 8.46 x 10^4 V/m$^{\frac{1}{2}}$ respectively (20).

The roughness factor m, commonly between 0.5 and 0.7 for the marred and dusty wires of industrial precipitators, is in the same approximate range for the heavily oxidized negative wires of the present tests (Figure 22). In every case, the negative corona starting field is well below the value for smooth clean wires. The positive starting fields (Figure 23) also show wide variability but, following expectation (19), are scattered over a somewhat narrower range closer to Peek's predicted values.

Current-Voltage Elbows

The elbow-like bends appearing close to corona onset in the negative current-voltage curves (e.g. Figures 12(e) and (f) and 13(e) and (f)) are also observed in room-temperature air at elevated pressures (19). This phenomenon, at least in the case of the sharply angular elbows, seems restricted to the negative discharge, and is more likely for larger diameter wires (cf. Figures 12(d), (e) and (f) and 13(d), (e) and (f)) and higher temperatures (usually for 1089 K and above). It might be supposed that surface asperities play a central part in initiating the very low current portion of the discharge. If these superficial irregularities consist of fine points of effective diameter less than that of the wire, a measurable corona current might be expected to flow at voltages below those anticipated on the basis of the nominal wire diameter. Such fine points would have a more pronounced effect, the larger the diameter of the wire relative to the size of the points.

Possibly, however, the explanation of the elbows is to be sought elsewhere. Field emission, the next mechanism to come to mind, requires fields greater than about 10^7 V/m, and then only if a suitably contaminated cathode surface is provided. The fact that some of current-voltage curves extend to, or close to, the origin of coordinates clearly excludes field emission from

further consideration. The preceding objection is conceivably met by postulating thermionic emission from the cathode, a mechanism which also possesses the advantage of accounting for the appearance of the elbows -- in this study -- only at high temperatures. Thermionic emission can yield significant currents at very low fields, at temperatures over 1000 K, provided that a suitable prepared and preserved emitting surface is available. That the essential combination of propitious circumstances might occur together by chance, in air, is altogether unlikely. The question of the origin of the elbows remains unanswered.

DISCHARGE ELECTRODE OSCILLATIONS

Seven discharge electrode geometries have been tested to determine (1) tendency to oscillate and (2) weight required to dampen oscillations without exceeding the yield stress point. These results are tabulated in Table 5 and include wire shape, size, length, weight ratio (w), temperature, sparking voltage, oscillation span and change in length. The parameter w is the ratio of the weight of electrode plus bottom weight to the electrode weight alone, and determines the applied tension. The oscillation span is the maximum swing of the discharge electrode toward the pipe. Peak and average sparking voltages are given for both polarities.

The large oscillations that are observed with the smaller diameter electrodes are successfully damped by increasing the weight ratio. The barbed wire, however, exceeds its yield stress point before being totally damped. Comparing the electrodes, the shorter lengths of 3.20 meters are found to exhibit less oscillation. The more rigid electrodes of larger diameter have a smaller oscillation span. Based on these results, a short rigid electrode, either twisted square or stranded, with its higher mechanical strength and low oscillation tendency, would be preferred to a small-diameter and long electrode. Oscillations are minimized by limiting the electrode lengths to 3 or 4 meters and using a relatively high weight ratio of between 10 and 15 total grams per gram of electrode.

MATERIAL EVALUATION

The surface roughness of the discharge electrode is a critical parameter for corona-starting and sparkover voltage. Oxidation that produces an expanding scale changes the starting voltage. Too deep an oxidation produces poor mechanical strength. Electrodes of 316 stainless steel produce severe oxidation scaling and are unsuitable for high-temperature operation. Inconel 600 produces a small increase in wire diameter after two weeks of cycling between 811 K and 1366 K. This material may be suitable at temperature levels of between 1000 K and 1250 K.

Table 5.

DISCHARGE ELECTRODE OSCILLATION RESULTS

Electrode Description	W Ratio	Length m.	Electrode Wt/Length q/m	Temp K	SPARKING VOLTAGES WIRE POLARITY Positive kVp	Positive kVavg	Negative kVp	Negative kVavg	Electode Oscillations cm Pos.	Neg.	Change In Electrode Length cm Pos.	Neg.	Resistance of Electrode ohm/m. @ 300 K
A. 7.94 mm	2.8	4.31	320.3	302	58.2	47.1	96.5	71.4	0	0	0	0	13.1×10^{-3}
Twisted Square	2.8	4.31	320.3	866	63.5	46.4	95	63.5	3.2-6.4	3.2-6.4	50.0	57.2	" "
(Magnetic)	2.8	4.31	320.3	1033	59.7	43.7	90	60.8	3.2	3.2-4.8	57.2	59.1	" "
	2.8	4.31	320.3	1089	60	43.3	93.8	62.3	0	0	63.5	69.9	" "
	2.8	4.31	320.3	1200	60	42.6	90	61.9	0	0	76.2	76.2	" "
	3.3	3.20	320.3	1366	60	42.9	90	60.3	0	0	47.6	50.8	" "
	3.3	3.20	320.3	303	55.5	44.1	100	74.6	0	0	0	0	" "
B. 6.35 mm	4.2	4.26	177.5	302	59	47.1	96.5	69.2	0	0	0	0	36.1×10^{-3}
Twisted Square	4.2	4.26	177.5	866	65	46.8	95	64.0	1.6-3.2	1.6-3.2	44.5	44.5	" "
(Magnetic)	4.2	4.26	177.5	1033	65	46.0	95	63.2	1.6-3.2	1.6-3.2	44.5	54.0	" "
	5.3	3.20	177.5	1200	63.5	45.4	95	66.1	0	0	50.8	50.8	" "
	5.3	3.20	177.5	302	55	44.5	100	74.5	0	1.6	0	0	" "
C. 6.35 mm	3.3	4.31	243.7	301	53.1	47.5	100	74.5		3.2-6.4	0	0	29.5×10^{-3}
Round	3.3	4.31	243.7	866	65	47.1	90	61.2	12.7-19.1	6.4-12.7	47.6	47.6	" "
(Magnetic)	3.3	4.31	243.7	1144	60	42.9	90	60	6.4-12.7	3.2-6.4	54	54	" "
	4.2	3.20	243.7	1366	60	43.5	83.3	57.4	0	0	57.2	57.2	" "
	4.2	3.20	243.7	302	55	48.0	103.1	83.1	0	0	0	0	" "
D. 3-2.77 mm	8.7	4.30	143.3	303	56.8	47.3	100	74.1			0	0	131×10^{-3}
Twisted Round	8.7*	4.30	143.3	866	64	46.2	75	53.4	12.7-19.1	50.8-76.2	57.2	57.2	" "
(Non-Magnetic)	11.4	3.20	143.3	1200-1255	62.9	45.8	100	68	0	0	63.5	66.7	" "
	11.4	3.20	143.3	305-299	55	45.6	97.3	74.1	0	0	0	0	" "

DISCHARGE ELECTRODE OSCILLATION RESULTS

(Cont.)

Electrode Description	W Ratio	Length m.	Electrode Wt/Length g/m	Temp K	SPARKING VOLTAGES WIRE POLARITY Positive kVp	Positive kVavg	Negative kVp	Negative kVavg	Electrode Oscillations cm Pos.	Electrode Oscillations cm Neg.	Change In Electrode Length cm Pos.	Change In Electrode Length cm Neg.	Resistance of Electrode ohm/m. @ 300 K
E. 6.35 mm Stranded Cable (Non-Magnetic)	9.1	4.31	172.9	304	57.1	47.9			0		0	0	194×10^{-3}
	7.1	4.31	172.9	305			100	73.7		0		0	" "
	7.1	4.31	172.9	866	65	47.1	85	61.6	6.4-12.7	19.1-25.4	57.2	54	" "
	4.3	4.31	172.9	866	56	41.4			38.1-50.8		41.3		" "
	7.1	4.31	172.9	1033	65	47.1	85	60	3.2	12.7-19.1	73.0	66.7	" "
	4.3	4.31	172.9	304	56	47.5			3.2				" "
	9.5	3.20	172.9	300	55	47.6	100	74.6	0	1.6			" "
	9.5	3.20	172.9	1200	64	45.6			0		73.0		" "
	9.5	3.20	172.9	1144			99.1	68.8		0		66.7	" "
F. 2.77 mm Round (Non-Magnetic	29.1	4.30	49.53	302	66.1	50.9			50.8		0		272×10^{-3}
	25	4.30	49.53	303			100	72.2				0	" "
	29.1	4.30	49.53	866	60	46	60	43.7	76.2-101.6	76.2-127	47.6	50.8	" "
	38.7	3.20	49.53	304	59.5	47.7			0		0		" "
	38.7	3.20	49.53	1061	65	47.1			9.5-19.1		34		" "
	30.9	3.20	49.53	302			110.6	81.8		19.1-25.4		0	" "
	30.9	3.20	49.53	1089			90	65		12.7-19.1		57.2	" "
G. two-1.59mm with 19mm barbs Barbed wire	7.5**	4.32	87.31	300	45	34.2			0		0		
	14.3***	4.32	87.31	300-303	50	37.4	80	57	0	0	0	0	
	14.3	4.32	87.31	866	50	36.5	75	52.9	101.6-127	3.2	41.3	41.3	
	14.3	4.32	87.31	922	55	39.5	75	52.4	25.4-38.1	3.2	41.3	41.3	

*W ratio = 5.0 for positive polarity
**Electrode weight not sufficent to hang straight
***Weight exceeded yield stress point

Inconel 601 produces an oxide coating 0.10 mm deep while being used at temperatures as high as 1400 K. The coating does not appear to change the wire diameter. Inconel 601 proved itself acceptable for use in these tests. Further experience under actual field conditions is required for long-term evaluation.

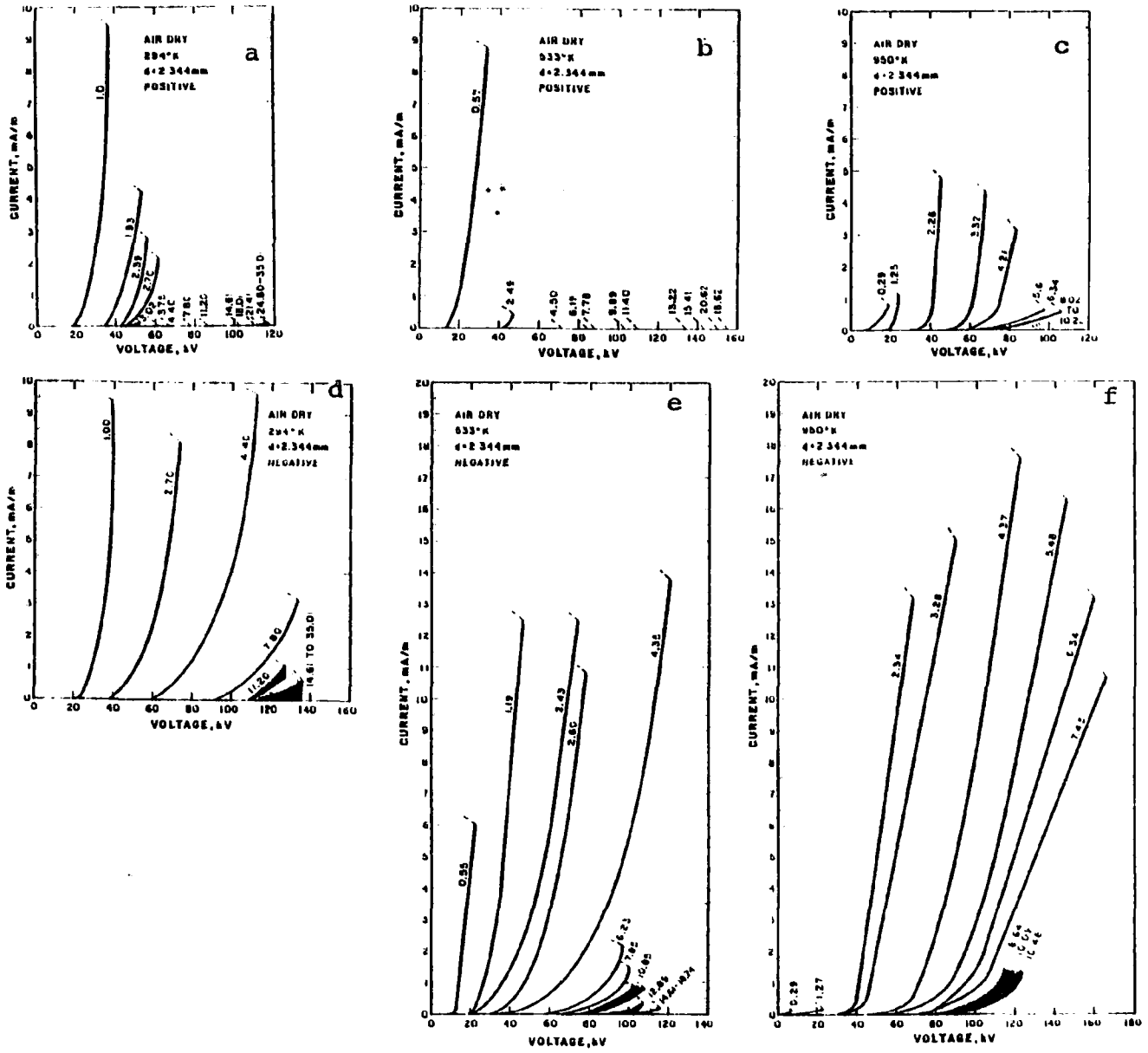

Figure 10. Current-Voltage Curves Taken in Dry Air at Temperatures of 294 K, 533 K, and 950 K for a 2.344 mm Wire Electrode.

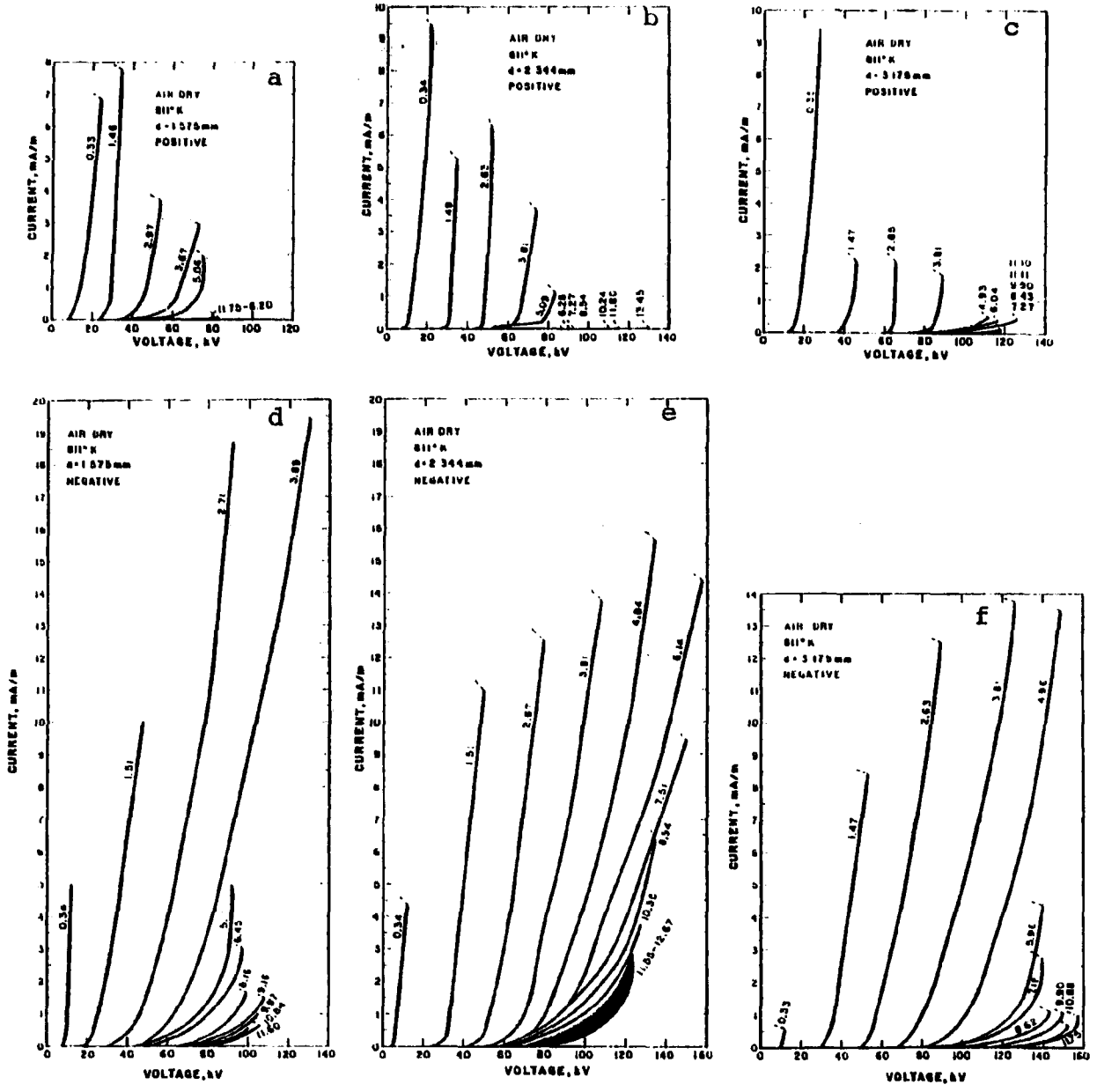

Figure 11. Current-Voltage Curves Taken in Air at a Temperature of 811 K for Wire Electrodes of 1.575mm, 2.344mm, and 3.175mm.

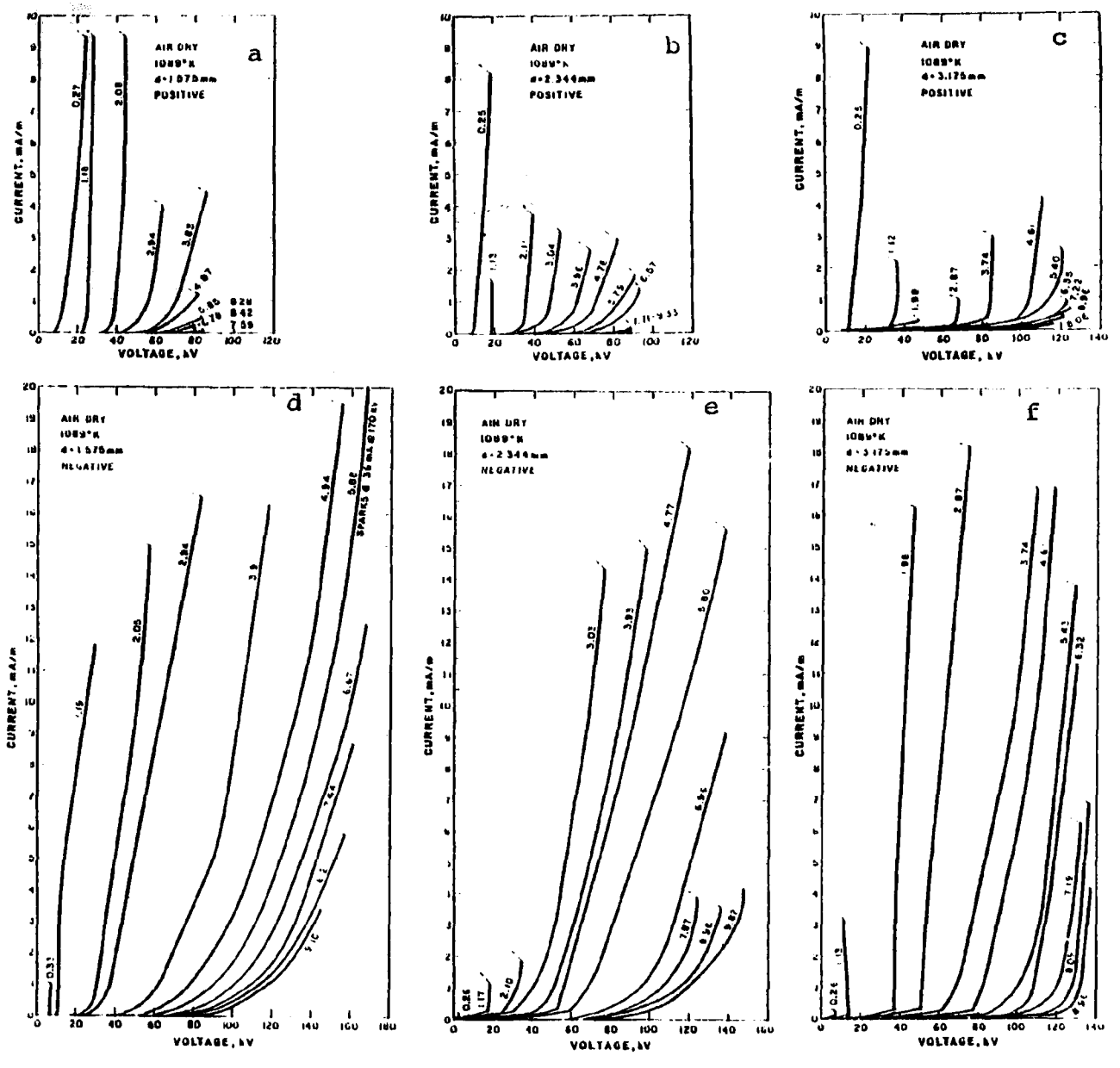

Figure 12. Current-Voltage Curves Taken in Air at a Temperature of 1089 K for Wire Electrodes of 1.575mm, 2.344mm, and 3.175mm.

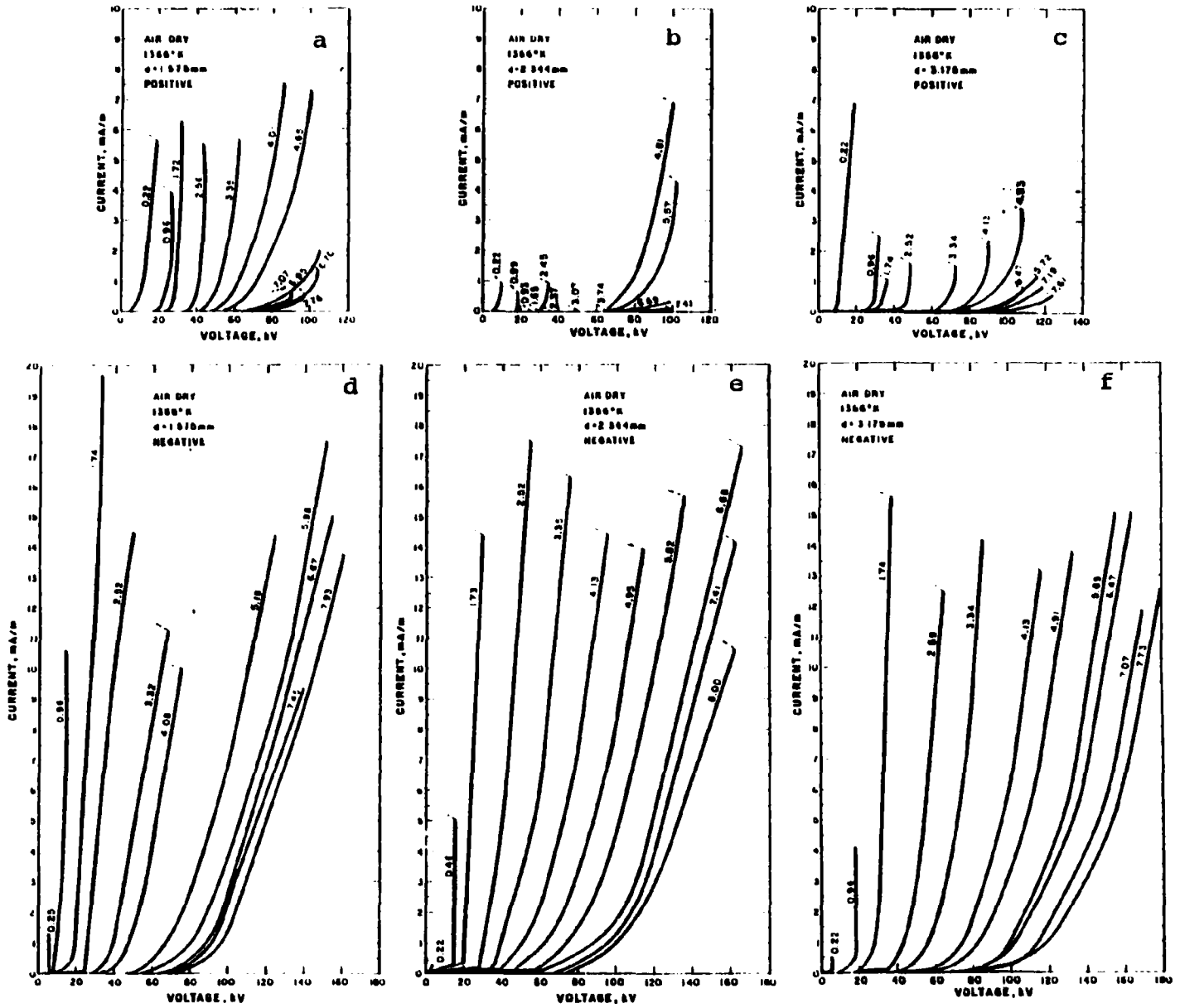

Figure 13. Current-Voltage Curves Taken in Air at a Temperature of 1366 K for Wire Electrodes of 1.575mm, 2.344mm, and 3.175mm.

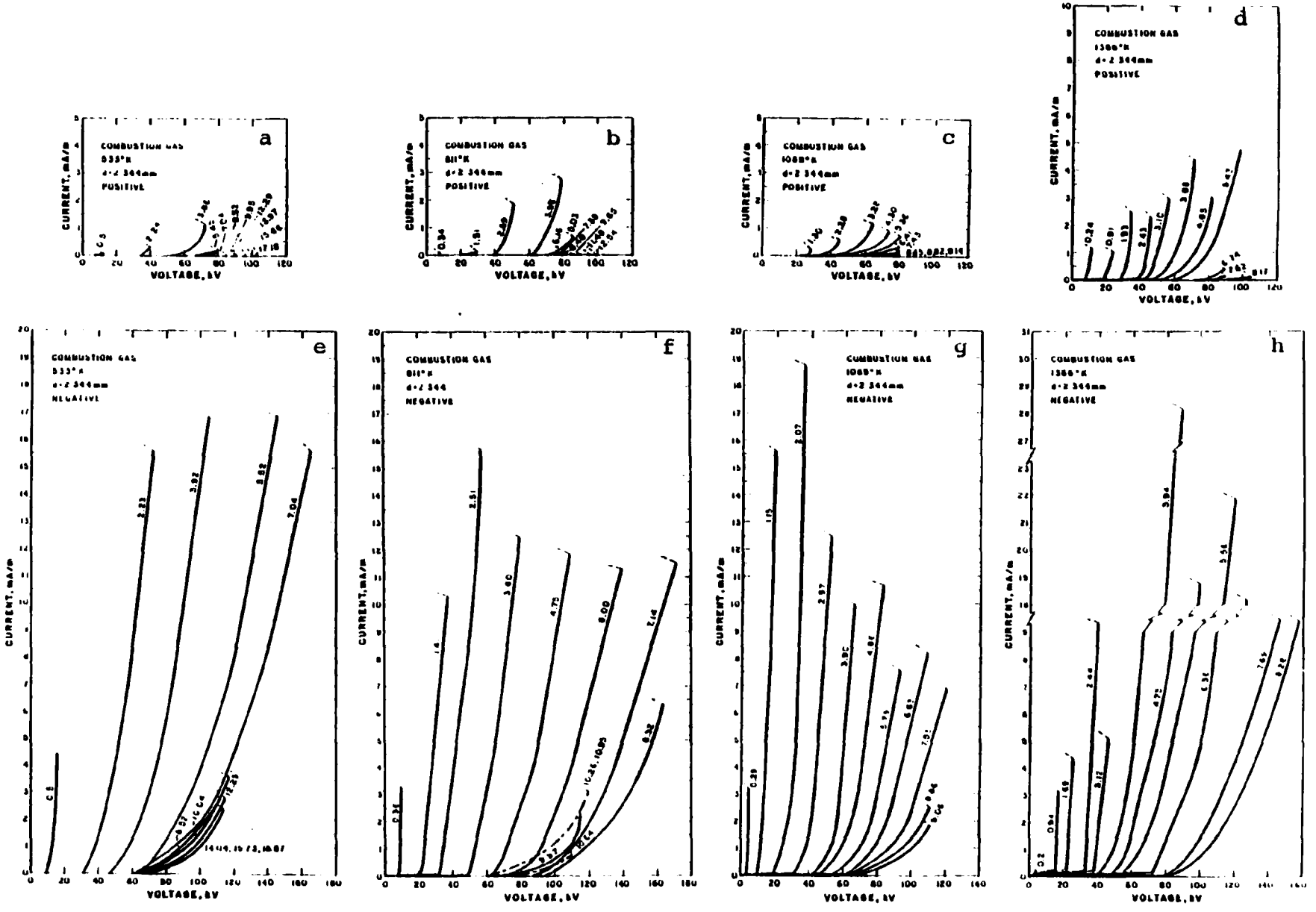

Figure 14. Current-Voltage Curves Taken in a Simulated Combustion Gas Mixture for Temperatures of 533 K, 811 K, 1089 K, and 1366 K Using a 2.344mm Wire Electrode.

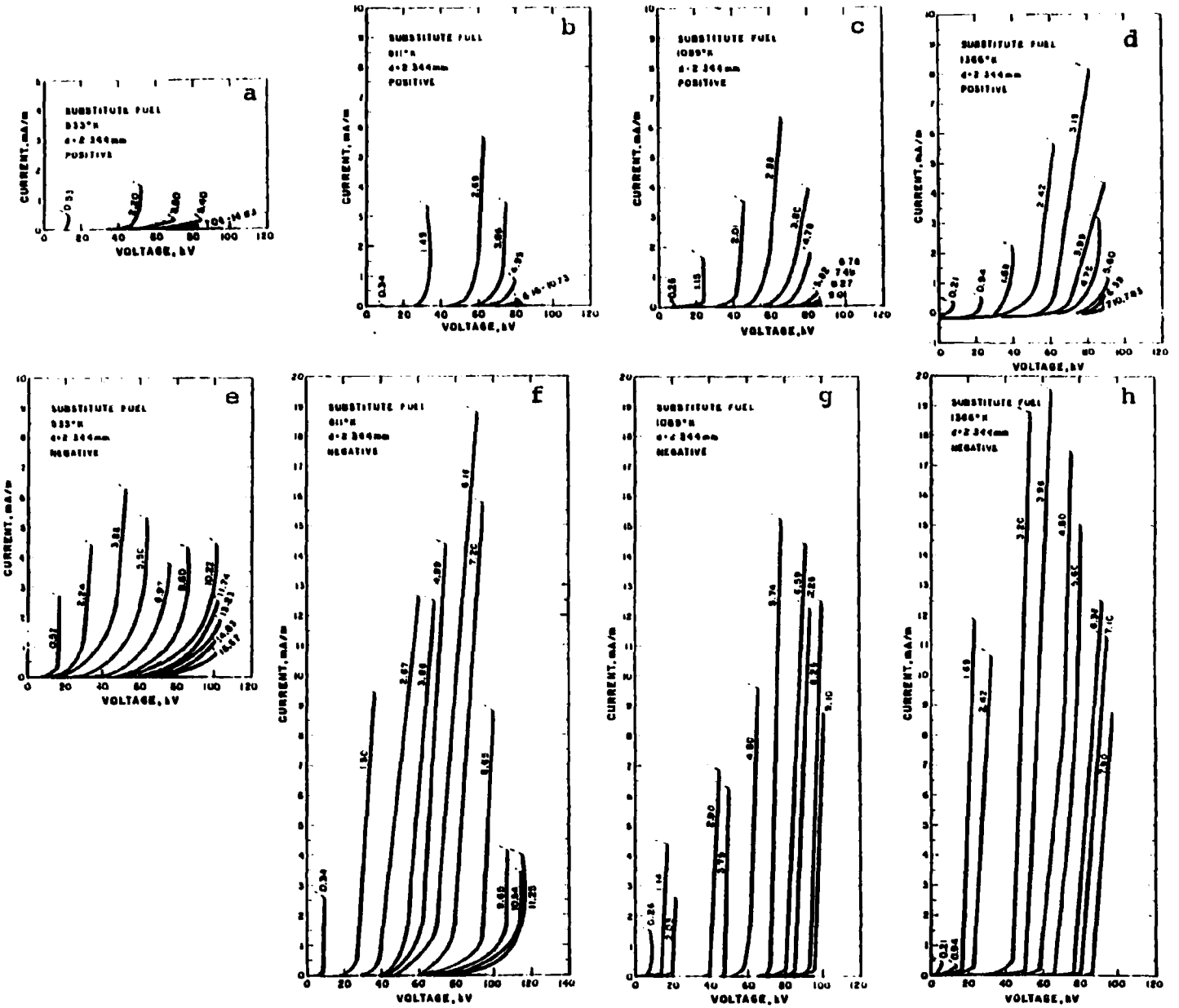

Figure 15. Current-Voltage Curves Taken With a Substitute Fuel Gas Mixture at Temperatures of 533 K, 811 K, and 1366 K for a 2.344mm Wire Electrode.

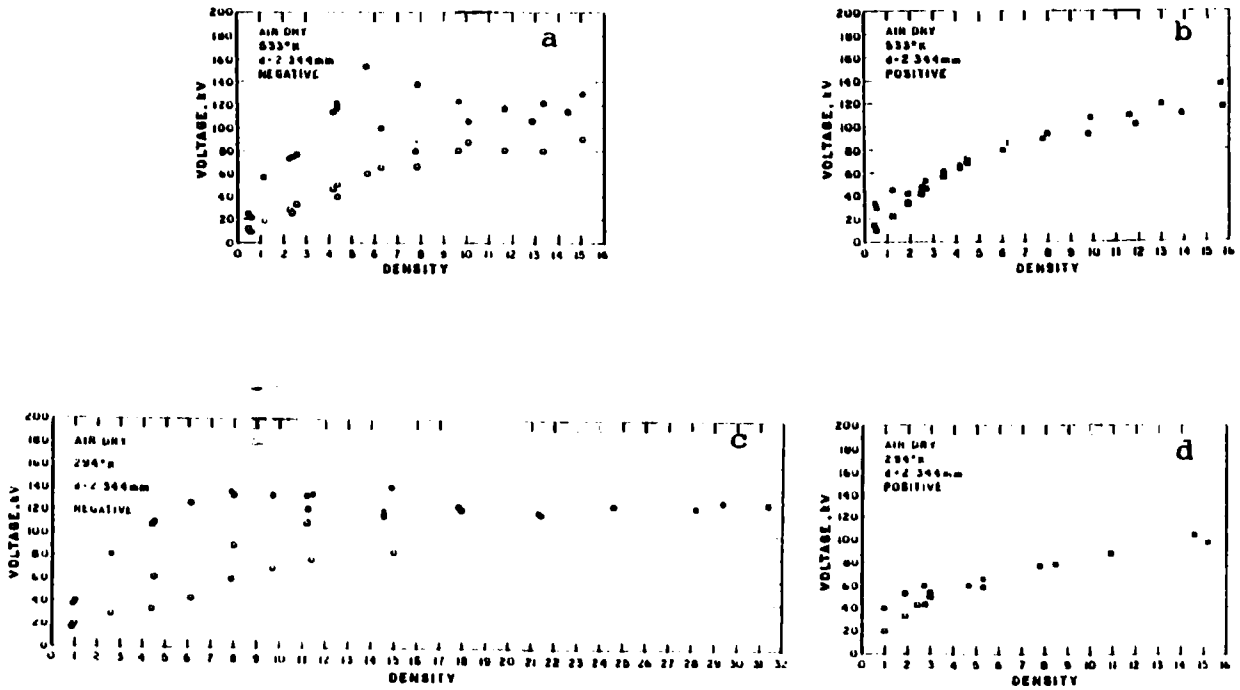

Figure 16. Sparking and Corona Starting Voltage in Air as a Function of Relative Air Density at 294 K and 533 K.

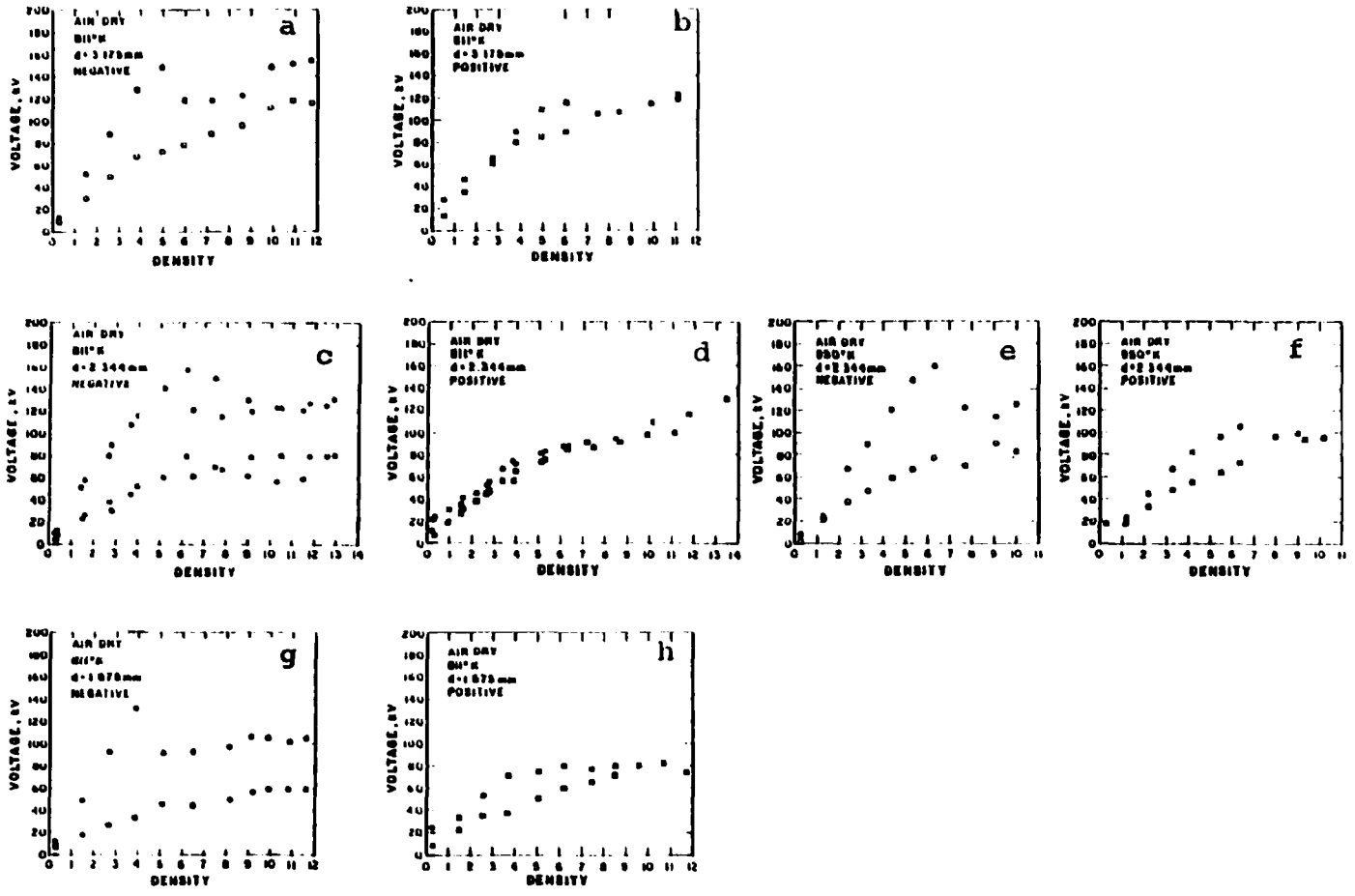

Figure 17. Sparking and Corona Starting Voltages in Air as a Function of the Relative Air Density at 811 K and 950 K for Wire Electrodes of 3.175mm, 2.344mm, and 1.575mm.

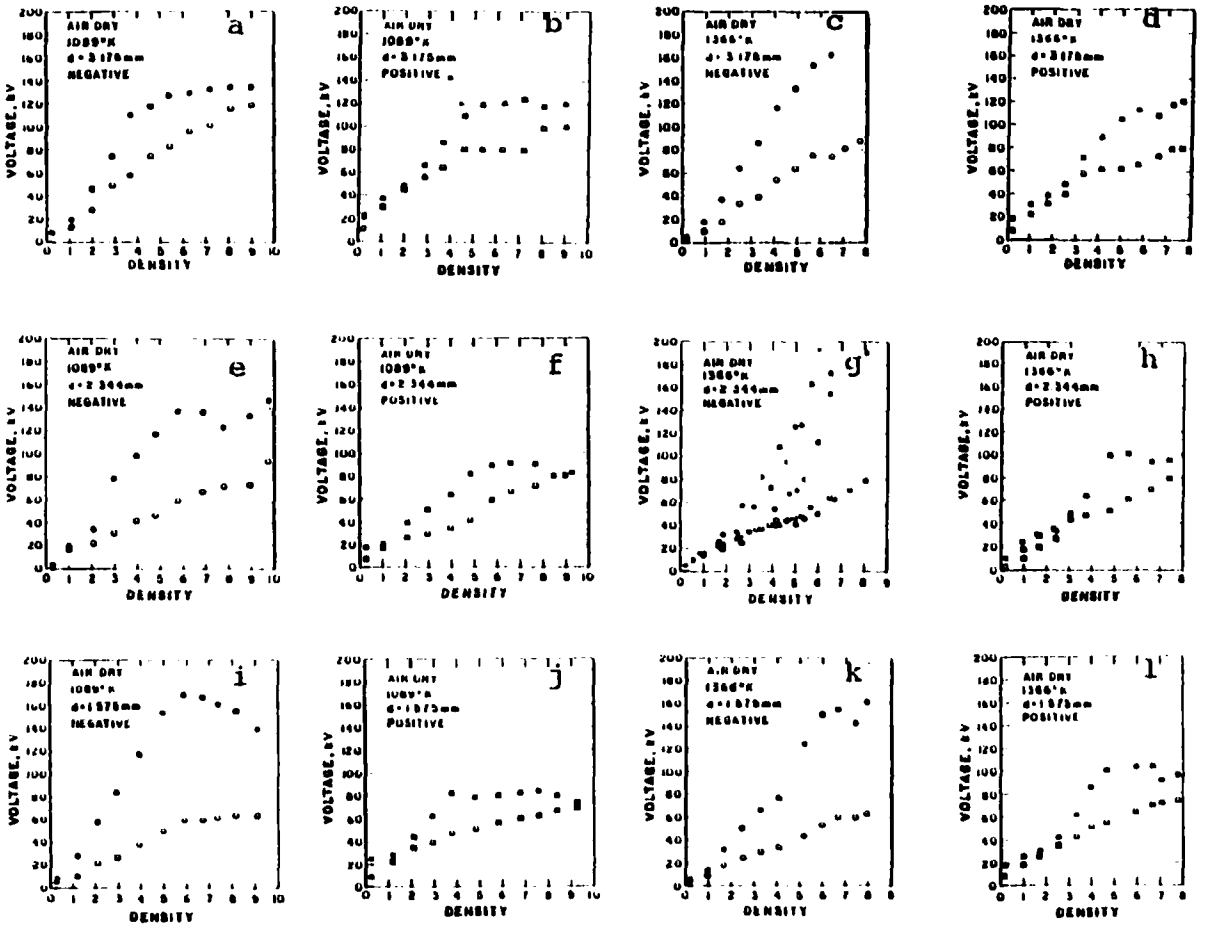

Figure 18. Sparking and Corona Starting Voltages in Air as a Function of Relative Air Density at 1089 K and 1366 K and for Wire Electrodes of 3.175 mm, 2.344mm, and 1.575mm.

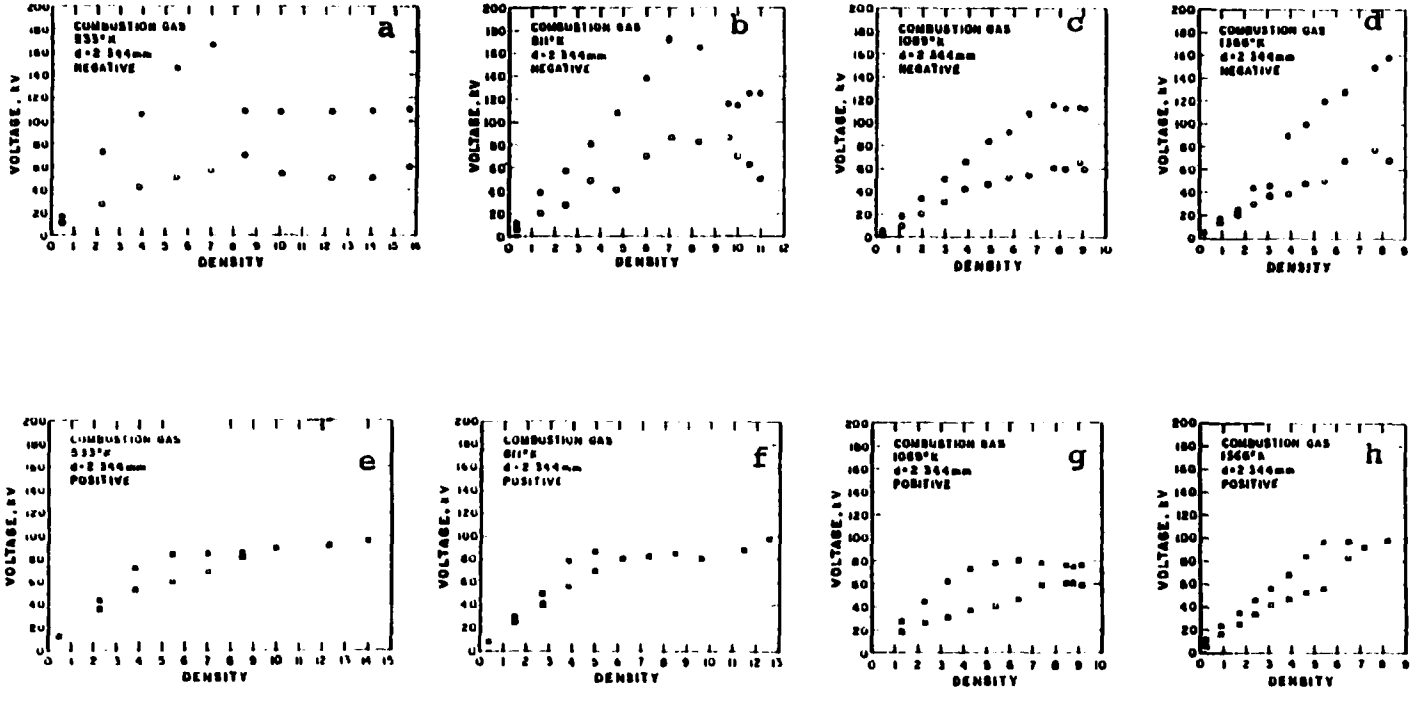

Figure 19. Sparking and Corona Starting Voltages for a Simulated Combustion Gas Mixture as a Function of Relative Gas Density at 533 K, 811 K, 1089 K, and 1366 K for a 2.344mm Wire Electrode.

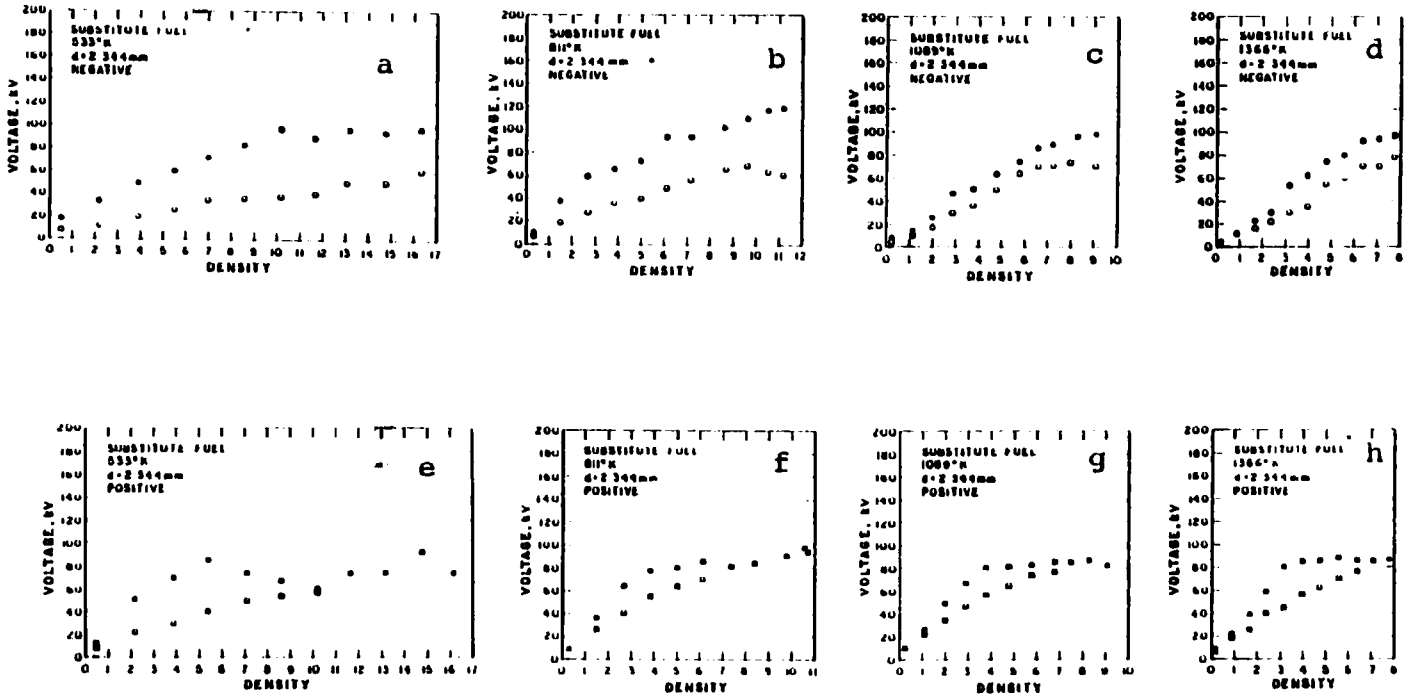

Figure 20. Sparking and Corona Starting Voltages in a Substitute Fuel Gas Mixture as a Function of Relative Gas Density at 533 K, 811 K, 1089 K, and 1366 K for a 2.344mm Wire Electrode.

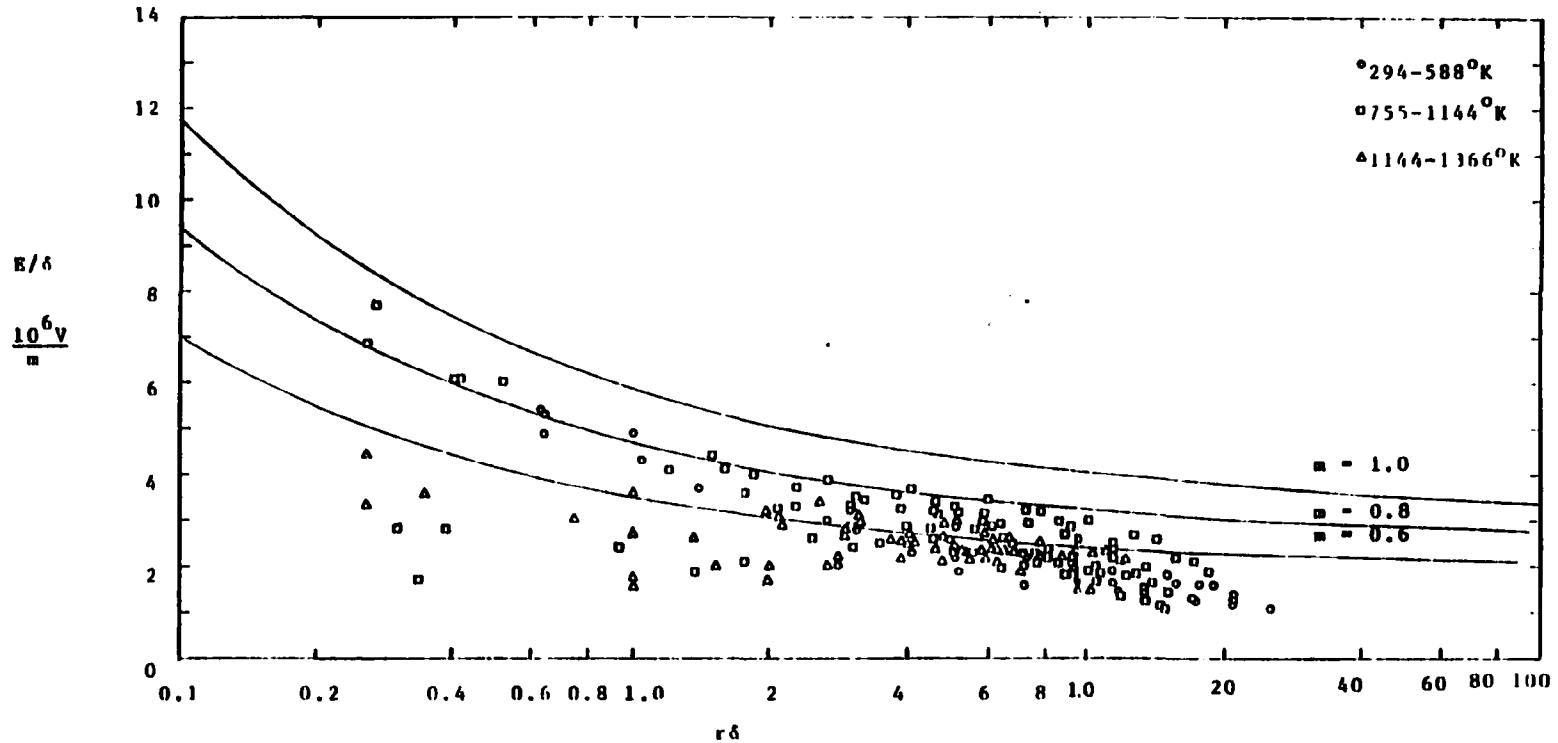

Figure 21 Corona Starting Field in Air for Negative Polarity and Compared with Peek's Equation for m = 1.0, 0.8, and 0.6.

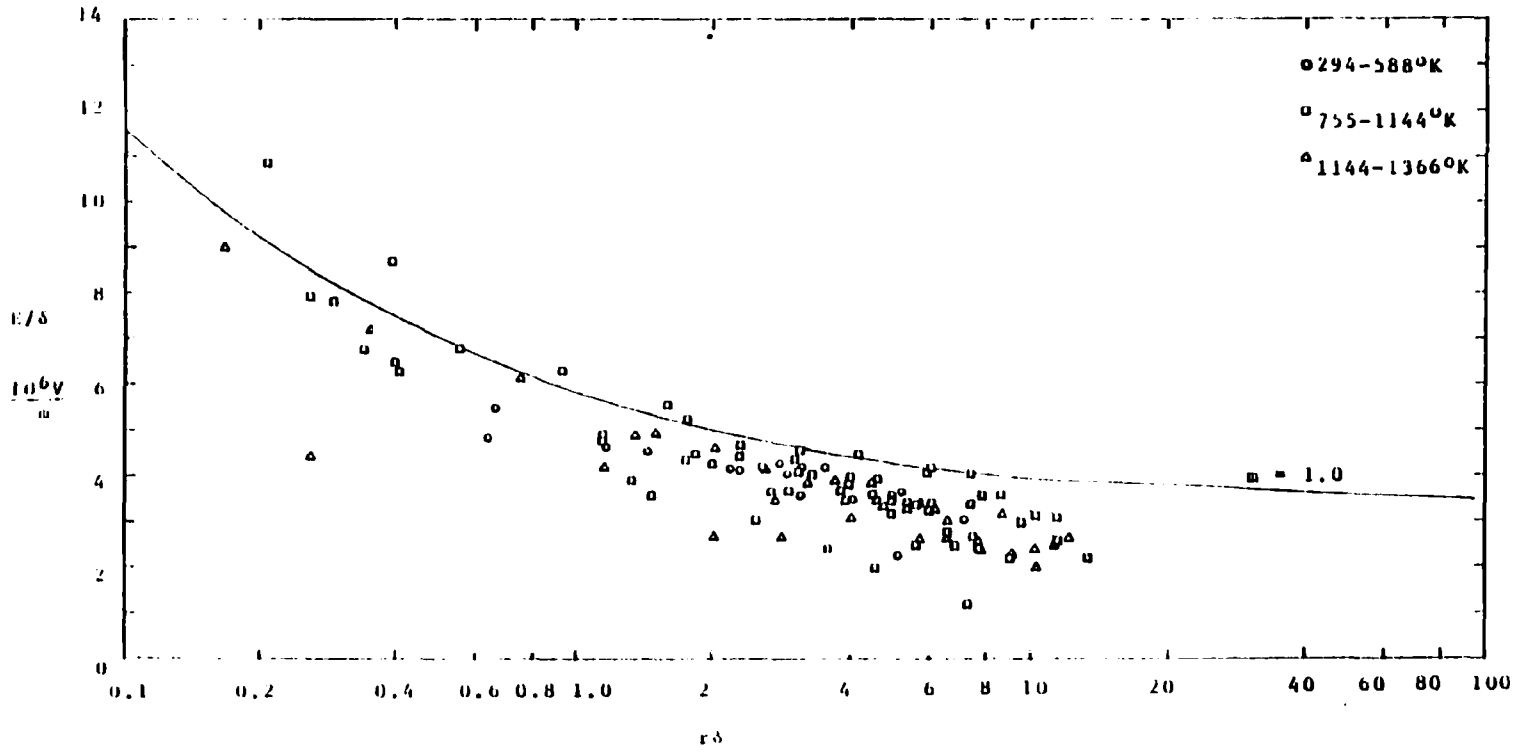

Figure 22 Corona Starting Field in Air for Positive Polarity Compared with Peek's Equation for m = 1.0.

SECTION 6

COMMERCIAL COST ESTIMATE

PRECIPITATOR SIZE FOR FLUIDIZED-BED COMBUSTION

The estimation of a practical size for a high-temperature, high-pressure electrostatic precipitator to clean the gases from a commercial fluidized-bed combustion unit follows seven steps.

1. Determination of the relationship between the gas flow rate (m^3/s) and power rating (MW).

2. Determination of the size of a commercial unit and its division into boiler modules.

3. Determination of the number of precipitator pipes required to serve each boiler module.

4. Determination of the vessel size for the given number of pipes and sub-multiples of that number.

5. Determination of the vessel thickness and estimated weight for each size.

6. Determination of the transformer-rectifier capacity required to serve each size.

7. Selection of the most practical size or sizes.

The details of these steps follow.

1. The relationship between the power rating and gas flow rate is derived from data for two pilot plants and one demonstration unit. These three sets of figures provide an estimated requirement of 0.661 m^3/s or 560 ACFM per each megawatt of generating capacity. See Table 6.

2. Two sizes are estabished for commercial fluidized bed combustion units, 300 MW and 600 MW. Since the 600 MW unit is double the size of the 300 MW unit, the 300 MW unit is considered.

Any requirements for this size can be doubled for the 600-MW unit. The 300-MW unit consists of four boiler modules and two gas turbines. Each boiler module consists of four stages of fluidized beds with embedded boiler tubes.

The logical arrangement is to have one or more precipitators serve each boiler module. The capacity per module is 75 MW. The estimated gas flow is:

$75 \times 0.264 = 19.8\ m^3/sec.$ (Actual)

or $75 \times 560 = 42{,}000$ ACFM

3. The gas flow capacity of each precipitator pipe is based on a treatment velocity of 1.52 m/sec. The pipe size is assumed to be 0.229 inside diameter x 3.05 m. The cross-section of 0.229 m pipe is 0.041 m^2. Multiplying by 1.524 m/sec equals 0.0625 m^3/sec per pipe. A gas flow rate of 19.81 m^3/sec requires 317 pipes. The relationship between the number of precipitators per boiler module and number of pipes per precipitator is shown in Table 7.

The expected efficiency of the precipitator(s) is 98 to 99 percent, based on a migration velocity of 0.122 m/sec. This migration velocity is estimated from the results of this report.

using the equation

$$w = \frac{\varepsilon_o d_p E_{av}^2}{\mu}$$

where:

w = migration velocity (m/sec)

ε_o = permittivity of free space (F/m)

d_p = mean particle diameter (m)

E_{av} = average electric field in pipe (V/m)

μ = gas viscosity (decapoise)

At conditions of 1089°K and 1000 kPa, the gas viscosity is approximately 4.1×10^{-5} decapoise, and from Figure 19f, the clean gas maximum field strength can be calculated to be about 1.5×10^6 V/m. If it is assumed that in the operating precipitator only half of this field strength can actually be realized, and that the mean particle size is only one micron, the indicated value of w = .122 results. It is felt that this estimated value of w is, therefore, conservative.

4. In order to determine the size of the vessel required for the various numbers of pipes, it is necessary to establish specific parameters. First, it is decided that 0.229-m diameter pipes require 0.305 m spacing, center to center. A minimum of 0.178 m is established as the clearance from the center of a pipe to the inside of the refractory lining of the vessel. This distance is needed for electrical clearance. The thickness of the refractory is estimed at 0.229 m. Preliminary design calculatio determine that the steel thickness of the pressure vessel is approximately 5.21 mm for each meter of vessel diameter.

Using these parameters, a simple computer program is used to find the relationship between vessel diameter and number of pipes. See Table 7.

5. The relationship of 5.21 mm of steel thickness to one meter of vessel diameter is based on an allowable steel stress 87,220 kPa (1). An internal pressure of 10 atm or 1010 kPa is used for design. The steel temperature is assumed to be no more than a few hundred degrees.

The estimated area of the vessel is based on a cylindrical shell, 4.88 m high. The 4.88 figure allows for the 3.05- m pipes plus 0.914 m top and bottom. The top is assumed to be a dished head. The bottom is conical with a slope of approximately 56 degrees with the horizontal.

6. The size of transformer-rectifier units plays a large part in establishing the practical-size precipitator. Most precipitators can be divided into small bus-sections and can be energized by any number of transformer-rectifiers. However, because of the high temperatures, these precipitators present special problems.

The high-voltage system is supported from insulators which are, in turn, supported by the pressure vessel. The collecting pipes are supported by a header plate inside the precipitator. When the precipitator is in operation at high temperature the header plate and wire support frame expand. The pressure vessel does not expand. Since the header plate and the wire support frame are intentionally made of the same material, it can be assumed that they will expand a like amount. However, if the wire support frame is supported from the insulators in an unsymmetrical manner, it will shift as it expands. This shift will throw the precipitator out of alignment. The discharge electrodes will no longer be in the center of the collecting pipes and the collection efficiency of the precipitator will be seriously impaired. As long as the wire support frame is symmetrically supported, it should not shift. It the wire support frame is divided into two or more parts, it must be unsymmetrical.

Based on the above, it is necessary for the precipitator to have a single wire support frame and, thus, be energized by a single transformer-rectifier unit. It is estimated that the current requirement per unit length of discharge electrode is approximately 3.28 mA/m. A precipitator with 317 3.05-m long pipes requires 3170 mA. The voltage is 150 kV peak or approximately 100 kV rms. With 3170 mA and 100 kV the power is 317 kW.

7. Almost any selection process is a process of elimination. First, the impossible choices are eliminated to obtain a list of possible alternatives. Table 7 represents this list. Next, the more undesirable choices are eliminated. This elimination is based on economics.

It can be assumed that 317 collecting pipes and discharge electrodes will cost the same, whether they are all in one precipitator or divided into many precipitators. Some elements, such as the header plate, are more costly in a large precipitator than in several smaller ones. Other items, such as the support insulators and insulator compartments, have a fixed cost per precipitator and thus increase as the number of precipitators increases. Up to about 3.6 or 4.0 m, a pressure vessel can be shop-fabricated. Beyond this size, shipping would become a problem. This factor works in favor of many small precipitators. While not a precipitator cost, the cost of the gas conveying systems affects the choice. In the absence of detailed information, it is not possible to be specific about these factors. It is estimated that the pluses and minuses tend to balance each other, with the fewer large precipitators having some advantage.

The one factor that can be estimated with some degree of accuracy is the weight of the pressure vessel. See section 5 above. The weight of each vessel is multiplied by the number of precipitators required. This figure is shown in the fourth column of Table 7. This determination combined with other higher costs eliminates the last four choices.

The choices are than narrowed down to two. The costs of these two sizes are estimated. The recommended size is one precipitator with 320 pipes. The two 160-pipe precipitators are in alternative selection. The details of these two selections are shown in Table 8.

MATERIAL-TEMPERATURE DEPENDENCE

At elevated temperatures, a small change in temperature can make a large difference in material selection. Characteristics that have no importance at moderate temperatures become critically important at high temperatures. These factors are also time-related factors which might not be sigificant on a short-term

pilot plant but would be very significant on a long-term commercial precipitator. Strength is also very drastically affected by temperature. Metals have a fairly uniform strength curve until a certain temperature. Above this temperature, the strength drops sharply. Thus, a slight increase in temperature could require much heavier structural sections. Thermal expansion also becomes very significant at high temperatures. At ambient temperature, it is frequently desirable to use different materials for different components. However, at high temperatures, slight differences in expansion rates could cause high stresses in materials that are welded together. If components are bolted together, different materials can be used.

The components are divided into two categories. The first category are those components where structural strength is less important but where scaling is the prime consideration. These components include the collecting pipes, the discharge wires, and the liner for the hopper bottom. The second category are those components where scaling is less significant but where structural strength and creep rupture are the prime consideration. These components include the header plate, the high voltage support system, and the pipe rapping frames.

The basic categories of materials are considered: stainless steels, andnickel and chromium alloys such as Inconel. The stainless steels are less expensive than the Inconels and, thus, are preferred where technically acceptable. However, the strength of these materials begins to drop sharply at 1089 K. Above 1144 K their strength is so poor that the savings per pound would be offset by the added quantity required. For this reason, stainless steels are recommended only up to 1144 K. Type 310 stainless is selected for the first category of components as it has better resistance to scaling. Type 316 stainless is selected for the second category of components because of its better creep rupture strength.

Above 1144 K up to 1311 K the use of Inconel is recommended. Inconel 601 is selected for the first category of components because it has good resistance to scaling. Inconel 617 is selected for the second category of components because it has the best creep rupture strength. Above 1311 K, the selction of materials becomes a very difficult problem.

The costs of precipitators in Table 8 is divided into Alternate A and Alternate B. Alternate A comprises precipitators with stainless-steel internals for operation up to 1144 K. Alternate B consists of precipitators with Inconel internals for operation from 1144 K to 1311 K. These costs are for equipment only and do not include erection.

Table 6

Unit	Combustion Power	Exxon	American Electric Power	Estimated Commercial
Power Rating (MW)	1	0.63	60	
Temperature (K)	1089	1089-1200	1172*	1172*
Pressure (kPa)	410	1000	1000	1000
Gas Flow (m^3/s)	1 - 1.5	0.3 - 0.4	40	--
(SCFM)	2120-3180	636 - 848	84,744	--
(ACFM)	1960-2940	235 - 346	33,738	--
Gas Flow per MW				
(m^3/s)	1 - 1.5	0.48 - 0.63	0.67	0.66
(SCFM)	2120-3180	1009-1345	1412	1400
(ACFM)	1960-2940	373 - 549	560	560

* Assumed

Table 7

Precipitators per Module	Pipes per Precipitator	Vessel Diam. (m)	Weight of Vessels (10^3 kg)
1	317	7.0	52.8
2	159	5.2	51.4
3	106	4.4	53.3
4	80	4.0	55.0
5	64	3.7	57.4
6	53	3.4	56.6

Table 8

	Recommended	Alternate
Number of Precipitators per Boiler Module	1	2
Pipes per Precipitator	320	160
Pipe Size	0.229 x 3.05m	0.229 x 3.05m
Vessel Diameter	7.0	5.2
Vessel Height	10.7	9.1
Steel Thickness	0.038	0.029
Vessel Weight	52.8×10^3 kg	25.7×10^3 kg
Capacity m^3/sec	19.82	9.91
ACFM	42,000	21,000
SCFM	106,000	53,000
MW of plant capacity	75	37.5
Collecting surface area	$700.5 m^2$	$350.2 m^2$
Discharge electrode length	975.4 lin. m.	487.7 lin. m.
SCA $(\frac{m^2}{m^3/sec})$	35.3	35.3
$(\frac{ft^2}{10^3\ ACFM})$	180	180
Expected efficiency	98-99%	98-99%
Power Supply		
Voltage	150 kV	150 kV
Current	3000 mA	1500 mA

	Recommended	Alternate
mA/m Discharge Electrode	3.08	3.08
mA/m^2/ Collecting Surface	4.31	4.31
$Watts/m^3/s$	1.462×10^4	1.462×10^4
Watts/ACFM	6.9	6.9
Costs		
Per precipitator - less engineering		
Alternate A	$1,945,000	$1,020,000
Alternate B	$2,185,000	$1,170,000
Per 300 MW Plant - including engineering		
Alternate A	$7,980,000	$8,360,000
Alternate B	$8,940,000	$9,560,000
Per KW of plant capacity		
Alternate A	$26.60	$27.90
Alternate B	$29.80	$31.90

SECTION 7

REFERENCES

1. American Society of Mechanical Engineers, Boiler and Pressure Code," Section VIII, p. 102, 19

2. Blum, F. L., "Estimated Size of a Commercial Unit for Fluidized-bed Combustion," Research-Cottrell, Inc., Bound Brook, NJ, 1977.

3. Brown, R. F. and Walker, A. B., "Feasibility Demonstration of Electrostatic Precipitation at 1700°F" J. Air Pollution Control Assoc. 21, 617-620 (1971).

4. Clavert, S. and Parker, R., "Collection Mechanisms at High Temperature and Pressure," Symp. Particulate Control Energy Proc., Document EPA-600/7-76-010, NTIS, 1976.

5. Calvert, S. and Parker B., "Effects of Temperature and Pressure on Particulate Collection Mechanisms: Theoretical Review," Document PB-264 203, NTIS, 1977.

6. Cooperman, P., "Spontaneous Ionization of Gases at High Temperature, "Conference Paper 63-173, Amer. Inst. Elec. Engrs., 1963.

7. Cooperman, P., "Positive Polarity Operation of Electrical Precipitators," Conference Paper 63-172, Inst. Elec. Electron. Engrs., 1963.

8. Cooperman, P., "Spontaneous Ionization of Gases at High Temperature," Paper ES-MON-6, Inst. Electron. Engrs., 1971.

9. Cooperman, P., "Positive Polarity Revisited," Symposium on Changing Technology in Electrostatic Precipitation, Inst. Fuel (Australian Membership), Adelaide, Nov. 1974.

10. Ekert, E. A. "Conditions Which Influence Spark-Potential Values," Sibley J. Eng. 18, 391ff. (1904).

11. Hall, H. J., Brown, R. F., Eaton, J. B., and Brown, C. W., "Removal of Lube Fume Raises Line Efficiency," Oil Gas J. 66 (37), 109-117 (1968).

12. Howell, A. H., "Breakdown Studies in Compressed Gases," Trans, Am. Inst. Elec. Engrs. 58, 193-204 (1939).

13. Huntington Alloys, Inc., "High Temperature Alloys - Hot Performance Guide, " Publication JN-159, 1975.

14. Koller, L. R. and Fremont, H. A. "Negative Wire Corona at High Temperature and Pressure," J. Appl. Phys. 21, 741-744 (1950).

15. Loeb, L. B. University of California, Private Communication, 1967.

16. Lowe, H. J. and Lucas, D. H., "The Physics of Electrostatic Precipitation," Brit, J. Appl. Phys. Suppl. No. 2, S40-S47 (1953).

17. Peek, F. W. Jr., Dielectric Phenomena in High-Voltage Engineering, 3rd ed., McGraw-Hill, New York, 1929, pp. 78,81.

18. Rao, A. K., Schrag, M. P. and Shannon, L. J., "Particulate Removal from Gas Streams at High Temperature/High Pressure," Document PB-245-858, NTIS, 1975.

19. Robinson, M., "The Corona Threshold for Coaxial Cylinders in Air at High Pressures," IEEE Trans. Power App. Systems 86, 185-189 (1967).

20. Robinson, M., "Electrostatic Precipitation" in Air Pollution Control, W. Strauss, ed., Vol. 1, Wiley-Interscience, New York, 1971, pp. 227-335.

21. Robinson, M., "Critical Pressures of the Positive Corona Between Concentric Cylinders in Air," J. Appl. Phys. 40, 5107-5112 (1969).

22. Robinson, M., Unpublished data.

23. Robinson, M. and Brown, R. F., "Electrically Supported Liquid Columns in High-Pressure Electrostatic Precipitators." Atmos. Environ. 5, 895-896 (1971).

24. Ryan, H. J., "Conductivity of the Atmosphere," Sibley J. Eng. 18, 267ff. (1904).

25. Shale, C. C., "Electrostatic Precipitation at High Temperatures and Pressures," Paper 64-8, Air Pollution Control Assocl, 1964.

26. Shale, C. C., "The Physical Phenomena Underlying the Negative and Positive Coronas in Air at High Temperatures and Pressures," Int. Conv. Record, Inst. Elec. Electron. Engrs., Part 7, 1965.

27. Shale, C. C., "New Concept of Electron Detachment for Air in Negative Corona at High Temperature," U.S. Bureau of Mines Information Circular 8385, 1967.

28. Shale, C. C., "Progress in High-Temperature Electrostatic Precipitation, J. Air Pollution Control Assoc. 17, 159-160 (1967).

29. Shale, C. C., Bowie, W. S., Holden, J. H. and Strimbeck, G. R. "Feasibility of Electrical Precipitation at High Temperatures and Pressures," U.S. Bureau of Mines Report of Investigations 6325, 1963.

30. Shale, C. C., Bowie, W. S., Holden, J. H. and Strimbeck, G. R. "Charactertistics of Positive Corona for Electrical Precipitation at High Temperatures and Pressures," U.S. Bureau of Mines Report of Investigation 6397, 1964.

31. Shale, C. C., and Fasching, G. E., "Operating Characteristics of a High-Temperature Electrostatic Precipitator," U. S. Bureau of Mines Report of Investigation 7276, 1969.

32. Shale, C. C. and Holden, J. H., "The Role of Wire Size in Negative Electrical Discharge at High Temperature," IGA Group, Inst. Elec. Electron. Engrs., 1968.

33. Thomas, J. B. and Wong, E., "Experimental Study of dc Corona at High Temperatures and Pressures, " J. Appl. Phys, 29, 1226-1230 (1958).

34. United States Steel Corp., "Steels for Elevated Temperature Service," Dec., 1974.

35. Walker, A. B, and Frisch, N. W., "U.S. Design and Operation Experienced with Hot Electrostatic Precipitators on Coal-Fired Utility Boilers," Joint US/USSR Symposium on Control of Particulate Emission and Related Problems, Moscow, 1976.

36. Winkel, A. and Schuetz, A., "Electrical Separation of Finely Dispersed Iron Oxide Dust at High Temperatures with Staub 22, 343-359 (1962).

37. Zabolotny, E. R. McCarthy, D. J., Korosi, A., Kurh, R. and Trueblood R. C., "Purification of Hot Fuel Gases from Coal or Heavy Oil," Document EPRI 243-1, NTIS, 1974.

SECTION 8

APPENDICES

A. Calculation of Thermal Conductivity

The thermal conductivity of a gas mixture can be estimated from the conductivity of each pure component, its molecular weight, and its mole fraction in the mixture according to the equation:

$$k_{mix} = \frac{\Sigma\ y_i k_i (M_i)^{1/3}}{\Sigma\ y_i (M_i)^{1/3}}.$$

Values of the thermal conductivity for the pure components at 300 K have been obtained from the Handbook of Chemistry and Physics, section E2. Higher temperature values can be estimated using the reduced properties chart available in Perry's Handbook of Chemical Engineering, page 3-245. Values of thermal conductivity for the gas mixtures used are thus tabulated as follows:

TABLE A-1

EVALUATION OF THERMAL CONDUCTIVITY

FOR TEST GAS MIXTURES

Component	M_i	Fuel y_i	Combustion y_i	k_{300}	k_{530}	k_{800}	k_{1100}	k_{1350}
				mW/(m-K)				
CO_2	44	0.230	0.092	19.30	41.4	58.2	74.6	87.1
O_2	32	-	0.028	30.6	50.0	67.3	79.8	95.2
N_2	28	0.0535	0.830	30.0	46.2	62.0	77.4	89.0
He	4	0.185	-	173.4	253.0	353.0	447.3	523.3
H_2O	18	0.05	0.05	20.5	44.7	78.4	-	-
Air	(28.8)	-	-	29.9	-	-	-	-
Fuel Gas Mix	(26.8)	(1.00)	-	41.1	65.9	91.4	115.9	134.7
Comb. Gas Mix	(29.1)	-	(1.00)	28.4	45.8	62.5	77.0	89.0

A low Btu fuel gas would have a value calculated as below:

TABLE A-2

THERMAL CONDUCTIVITY OF A LOW-BTU FUEL GAS

Component	M_i	Y_i	k_{300}	
CO_2	44	0.087	19.1	mW/(m-K)
CO	28	0.174	28.8	
H_2	2	0.124	214.7	
CH_4	16	0.033	39.4	
N_2	28	0.482	30.0	
H_2O	18	0.10	20.5	
Fuel Gas	(24.8)	(1.00)	38.3	

B. Calculation of Ionic Mobility

Estimated values of ionic mobility b can be calculated using the equation:

$$\frac{1}{b_{mix}} = \Sigma(y_i/b_i)/\Sigma y_i$$

Values for the pure gas components have been taken from table 3 of Strauss : Air Pollution Control Part I, page 240. The following table summarizes the calculations for the gas mixtures tested and for a low Btu fuel gas.

TABLE B-1

IONIC MOBILITIES

Component	Actual Fuel y_i	Substitute Fuel y_i	Combustion y_i	$(m^2/(s-V)$ b_o^-	b_o^+
He	-	0.185	- -	16.7×10^{-4}	10.4×10^{-4}
N_2	0.482	0.185	0.83	2.27×10^{-4}	1.8×10^{-4}
O_2	-	-	0.028	2.46×10^{-4}	2.2×10^{-4}
CO_2	0.087	0.230	0.092	0.98×10^{-4}	0.84×10^{-4}
H_2	0.124	-	-	16×10^{-4}	12.3×10^{-4}
CO	0.174	-	-	1.14×10^{-4}	1.10×10^{-4}
H_2O	1.10	0.05	0.05	0.95×10^{-4}	1.10×10^{-4}
CH_4	0.033	-	-	0.8×10^{-4}	0.8×10^{-4}
Air	-	-	-	2.5×10^{-4}	1.8×10^{-4}
Fuel Gas	(1.0)	-	-	1.64×10^{-4}	1.49×10^{-4}
Substitute Fuel Mix	-	(1.0)	-	1.87×10^{-4}	1.58×10^{-4}
Com. Gas Mix			(1.0)	1.91×10^{-4}	1.59×10^{-4}

C. Gas-Mixture Composition as Determined From Partial Pressure and Mixing Procedure

Air

Compressed dry air containing less than 0.01% H_2O as obtained from the Matheson Gas Co. has been used directly to fill the pressure vessel from atmospheric conditions to 3550 kPa. The composition thus remains constant:

O_2 = 21%

N_2 = 79%

Combustion Gas

For combustion gas the vessel is first purged with nitrogen. Using a 77%-CO_2, 23%-O_2 gas mixture the vessel is filled from 101 kPa to 550 kPa, with the gas passing through the humidifier. The remainder of the gas -- N_2 -- fills the pressure vessel through the humidifier to a pressure of 3550 kPa. The humidifier saturates the gas at 388 K resulting in a 5% moisture content. The final composition of the gas can then be determined based on each components partial pressure: $\%(i) = 100 \dfrac{Pi}{P\ total}$

where Pi = Pressure increment x $\frac{\%i}{100}$ in gas added x $(1 - \frac{\%H_2O}{100})$

TABLE C-1

COMBUSTION GAS MIXTURE COMPOSITION

i		%
CO_2	$= \dfrac{(0.55-0.10) \times 10^6 \ (0.77)\ (1-0.05)}{3.55 \times 10^6 \times 100}$	= 9.2
O_2	$= \dfrac{(0.55-0.10) \times 10^6 \ (0.23)(1-0.05)}{3.55 \times 10^6 \times 100}$	= 2.8
N_2	$= \dfrac{(3.55-0.55 + 0.10) \times 10^6 \ (1.0)(1-0.05)}{3.55 \times 10^6 \times 100}$	= 83.0
H_2O	=	5.0

Substitute Fuel Gas

The fuel gas mixture is made by first purging with a 30% CO_2 - 70% N_2 mixture. All components are added through the humidifier - set to give a 5% moisture content. A three-step procedure is used for pressurizing: (1) Using 30% CO_2, 70% N_2 mixture, the vessel is pressurized to 1140 kPa; (2) Using helium the vessel is filled from 1140 kPa to 1830 kPa; (3) Using the 30% CO_2, 70% N_2 the gas is filled to a final pressure of 3550 kPa. Using the same calculation procedure as for combustion gas, a final composition of the substitute fuel gas can be determined:

TABLE C-2

SUBSTITUTE FUEL GAS MIXTURE COMPOSITION

i		%
H_2O		5
He	$= \frac{(1.83-1.14) \times 10^6 \ (1.0) \ (1-0.05)}{3.55 \times 10^6 \times 100} =$	18.5
CO_2	$= \frac{(3.55-1.83 \times 1.14) \times 10^6 \ (0.03) \ (1-0.05)}{3.55 \times 10^6 \times 100} =$	23.0
N_2	$= \frac{(3.55-1.83 \times 1.14) \times 10^6 \ (0.70) \ (1-0.05)}{3.55 \times 10^6 \times 100} =$	53.5

TABLE D

COMPONENTS OF POWER-SUPPLY CIRCUIT

C_1-C_{18}	capacitors	0.05 μF
C_{19}	capacitors	100 μF
C_{20}	capacitors	2 μF
C_{21},C_{22},C_{24},C_{25},C_{28}, C_{29}	capacitors	10 μF
C_{23},C_{26},C_{27}	capacitors	0.1 μF
CR_1 - CR_4	silicon-rectifiers	1000 mA, 260KV peak
j_1	oscilliscope jack plug	--
L_1	inductor coil - oil immersed	0.56 mH
L_2-L_4	inductor coil - air	4.7 mH
M_1-M_3	G.E. metal oxide variator	14 V
P_1-P_{12}	Variacs in rack	280V, 15A, each
R_1	resistor	20 k ohm
R_2	resistor	120 k ohm
R_3	resistor	207 M ohm
R_4	resistor	2 k ohm
R_5	resistor	5 k ohm
R_6	resistor	50 k ohm
R_7	resistor	5 k ohm
R_8	resistor	50 ohm
R_9	resistor	200 ohm
R_{10}	resistor	2.5 M ohm
R_{11}, R_{13}	resistor	10 k ohm
R_{12}	resistor	51.75 k ohm
R_{14}	resistor	10.35 k ohm
R_{15}	resistor	1.00 ohm
SP_1-SP_2	High Voltage Surge Protector - Carbon	400 V
SG_1	needle point spark gap	50 V
T_1	high voltage transformer	480 V to 106 V peak

TABLE E

RESEARCH-COTTRELL, INC.

LIST OF DRAWINGS FOR

HIGH PRESSURE/HIGH TEMPERATURE

PRECIPITATOR CES-273-P-001

Drawing No.	Rev.	Title
104855-L		Detailed Fabrication Specifications
104856-L		List of Drawings (this list)
104857-B		High Temp. High Pressure Precipitator Assembly
104858-B		Top Insulator Compartment Assembly & Details
104859-B		Top Insulator Compartment Details
104860-B		High Temp. High Pressure Precipitator Compartment Assembly and Details
104861-B		High Temp. High Pressure Precipitator Compartment details
104862-B		Bottom Insulator Compartment Assembly and Details
104865-B	2	High Temp. High Pressure Precipitator Pressure Vessels
104866-C		High Temp. High Pressure Precipitator Heater Bushings
104868-B		Heater Humidifier Assembly
104869-B		Heater Humidifier

RESEARCH-COTTRELL, INC.

SPECIFICATIONS FOR

HIGH PRESSURE/HIGH TEMPERATURE

PRECIPITATOR CES 273-P-001

1. SCOPE - This specification establishes the minimum requirements for the mechanical design, materials, fabrication, testing, inspection, and delivery of a high pressure/high temperature precipitator and its attachments and appurtenances.

2. RESPONSIBILITY - In applying this specification, and the details pertinent to the high pressure/high temperature precipitator, the seller accepts the full responsibility for the design, fabrication, and conformance to this document, referenced specifications, regulations, and purchase order.

3. REFERENCES - The latest edition or revision of the following references become part of this specification.

   ASME Boiler and Pressure Vessel Code

   Section I - Power Boilers
   Section II - Material Specifications
   Section VIII - Unfired Pressure Vessels
   Section IX - Welding Qualifications
   ANSI B16.5 - Steel Pipe Flanges and Flanged Fittings

4. CODE COMPLIANCE - Design, fabricate, and inspect the high pressure/high temperature precipitator in accordance with applicable sections of the ASME Code. Code stamp the precipitator and comply with all the acts and regulations of the jurisdiction in which the equipment is to be operated (Bridgewater Township, Somerset County, New Jersey).

5. DESIGN CRITERIA - Pressure shell code stamped in accordance with current ASME code section VIII for the following conditions:

Designed Operating Pressure	500 PSIG
Designed Operating Temperature	375°F
Hydrostatic Test	1000 PSIG
Joint Efficiency	100%

5. DESIGN CRITERIA (cont.)

All gaskets corrugated stainless steel, asbestos filled.

Flanges (ASTM A181-GRI)

Concentric reducer, 10" Ø pipe and 10" straight TEE (ASTM A515-70 or equal)

10 ga plate and 3/4" Ø std. pipe (ASTM A106-GRB)

Flange Bolting: ASTM A193GRB7 studs
ASTM A194GR2H nuts

Flange bolts to straddle centerlines.

Paint outside surfaces only with high temperature aluminum

6. CALCULATIONS - Prepare and submit all design and analysis calculations for review before fabrication starts. Include all references and assumptions. Calculations shall demonstrate equipment applicability for all design and operating conditions as delineated in the process diagram.

7. ATTACHMENTS - All attachments, internal and external, shall be designed and installed to leave no trapped void space behind the attachment.

8. CORROSION ALLOWANCE - Provide a 1/8 inch corrosion allowance for the shell, nozzles, and covers.

9. MATERIAL - All pressure sustaining parts shall be fabricated of carbon or low alloy steel. Internal parts shall be fabricated of stainless steel type 316 or INCONEL 600.

10. WELDING - Shall be in accordance with the American Welding Society latest revisions. Welding Stainless Steel to mild steel use A.W.S. A5.11 class E Ni Cr Fe-2 electrode. Welding Stainless Steel to Stainless Steel use A.W.S. ASTM E316L-16 electrode. Welding inconel 600 to inconel 600 use inconel coated rod #182 electrode.

11. QUANTITIES REQUIRED - The quantities required are as follows:

Qty.		
1	Top Insulator Compartment	104865-B1
1	Middle Precipitator Compartment	104865-B2
1	Bottom Insulator Compartment	104865-B3
1	Humidifer Heater Compartment	104865-B4

TECHNICAL REPORT DATA
(Please read Instructions on the reverse before completing)

1. REPORT NO. EPA-600/7-77-132	2.	3. RECIPIENT'S ACCESSION NO.
4. TITLE AND SUBTITLE Development of a High-Temperature/High-Pressure Electrostatic Precipitator		5. REPORT DATE November 1977
		6. PERFORMING ORGANIZATION CODE
7. AUTHOR(S) J.R. Bush, P.L. Feldman, and M. Robinson		8. PERFORMING ORGANIZATION REPORT NO.
9. PERFORMING ORGANIZATION NAME AND ADDRESS Cottrell Environmental Systems Research-Cottrell, Inc. Bound Brook, New Jersey 08805		10. PROGRAM ELEMENT NO. EHE623A
		11. CONTRACT/GRANT NO. 68-02-2104
12. SPONSORING AGENCY NAME AND ADDRESS EPA, Office of Research and Development Industrial Environmental Research Laboratory Research Triangle Park, NC 27711		13. TYPE OF REPORT AND PERIOD COVERED Final; 8/75-8/77
		14. SPONSORING AGENCY CODE EPA/600/13

15. SUPPLEMENTARY NOTES IERL-RTP project officer for this report is Leslie E. Sparks, Mail Drop 61, 919/541-2925.

16. ABSTRACT The report gives results of a laboratory test demonstrating the feasibility of electrostatic precipitation at high temperatures (to 1366 K) and pressures (to 3550 kPa): corona currents were stable at all temperatures. Detailed current/voltage characteristics under negative and positive polarity were obtained in dry air, in a simulated combustion gas, and in a substitute fuel gas for each temperature and pressure level. Major effects of temperature, pressure, and electrode geometry on precipitator design characteristics (sparking voltages, corona starting voltages, and current levels) were evaluated. This work has established that no practical temperature or pressure limitation exists to the levels tested. A preliminary cost estimate is presented for a commercial-size precipitator design applied to a commercial fluidized-bed combustor and turbine system.

17. KEY WORDS AND DOCUMENT ANALYSIS

a. DESCRIPTORS	b. IDENTIFIERS/OPEN ENDED TERMS	c. COSATI Field/Group
Air Pollution Electrostatic Precipitators High Temperature Tests High Pressure Tests	Air Pollution Control Stationary Sources	13B 14B

18. DISTRIBUTION STATEMENT Unlimited	19. SECURITY CLASS (This Report) Unclassified	21. NO. OF PAGES 81
	20. SECURITY CLASS (This page) Unclassified	22. PRICE

EPA Form 2220-1 (9-73)